

Time-dependent global sensitivity analysis of the Doyle-Fuller-Newman model

Elia Zonta^{a,*}, Ivana Jovanovic Buha^b, Michele Spinola^c, Christoph Weißinger^c, Hans-Joachim Bungartz^b, Andreas Jossen^a

^aTechnical University of Munich, School of Engineering and Design, Department of Energy and Process Engineering, Chair of Electrical Energy Storage Technology, Arcisstraße 21, Munich, 80333, Germany

^bTechnical University of Munich, School of Computation, Information and Technology, Department of Computer Science, Chair of Scientific Computing, Boltzmannstraße 3, Garching, 85748, Germany

^cCapgemini Engineering, Center of Excellence Battery, Frankfurter Ring 81, Munich, 80807, Germany

arXiv:2502.17275v2 [cond-mat.mtrl-sci] 31 Mar 2026

Abstract

The Doyle-Fuller-Newman model is arguably the most ubiquitous electrochemical model in lithium-ion battery research. Since it is a highly nonlinear model, its input-output relations are still poorly understood. Researchers therefore often employ sensitivity analyses to elucidate relative parametric importance for certain use cases. However, some methods are ill-suited for the complexity of the model and appropriate methods often face the downside of only being applicable to scalar quantities of interest. We implement a novel framework for global sensitivity analysis of time-dependent model outputs and apply it to a drive cycle simulation. We conduct a full and a subgroup sensitivity analysis to resolve lowly sensitive parameters and explore the model error when unimportant parameters are set to arbitrary values. Our findings suggest that the method identifies insensitive parameters whose variations cause only small deviations in the voltage response of the model. By providing the methodology, we hope research questions related to parametric sensitivity for time-dependent quantities of interest, such as voltage responses, can be addressed more easily and adequately in simulative battery research and beyond.

Keywords: Lithium-ion battery, Variance-based sensitivity analysis, Battery modeling, Uncertainty quantification, Parameter sensitivity, Sobol' indices

1. Introduction

Necessitated by the ongoing efforts to reduce carbon emissions and thereby mitigate the effects of climate change, lithium-ion batteries have become increasingly popular in the electrification of transport and the storage of renewable energy [1]. The intensification of battery research focused on improved energy density, lifetime, and optimal utilization therefore lies at the forefront of attenuating the impact of global warming by enabling a renewable energy transition and reducing greenhouse gas emissions.

Computational models are indispensable to many of the aforementioned research areas. Whether it be fast charging protocols [2], battery pack design for automotive applications [3], or the elucidation of dominant aging mechanisms [4], simulations enable the cost-efficient investigation of systems of interest, the estimation of internal quantities *in operando* and facilitate scientists to vary experimentally inaccessible control variables in numerical experiments.

However, the employed models in battery research tend to be very complex and comprise a large number of parameters. Arguably the most prominent electrochemical model for battery dynamics is the Doyle-Fuller-Newman (DFN) or pseudo-two-dimensional (p2D) model, conceived by the eponymous Doyle, Fuller, and Newman [5, 6]. It is composed of partial

differential-algebraic equations describing charge transport, mass transport, and electrochemical reactions. Researchers therefore often seek to reduce the complexity of these models and alleviate their parametrization by only considering the most influential model parameters. This has led to a substantial increase in conducted sensitivity analyses in battery research (Fig. 1). Sensitivity analysis aims at quantifying the impact of a parameter variation on the model output in the form of a sensitivity index, in order to obtain a relative importance ranking of the model parameters.

There exist various approaches to perform sensitivity analysis, but not all are equally suited for the evaluation of complex models. In fact, Saltelli et al. [7, 8] highlight misconceptions in a considerable number of published sensitivity analyses across numerous scientific disciplines. One of their biggest concerns is the application of one-at-a-time (OAT) methods to highly nonlinear models, which restricts the validity of the obtained results and hinders straightforward interpretation. In battery research, OAT methods are arguably the most prevalent practice for determining parametric sensitivity [9–21]. In light of the nonlinearity of the DFN model and similar battery models, this is a widely made but nonetheless suboptimal choice.

The use of global sensitivity analysis, i.e., methods suitable for nonlinear models, is comparatively scarce. Among the available methods, variance-based sensitivity analysis is probably the most commonly employed technique, besides the elementary effect test [22, 23], also known as Morris method.

*Corresponding author

Email address: elia.zonta@tum.de (Elia Zonta)

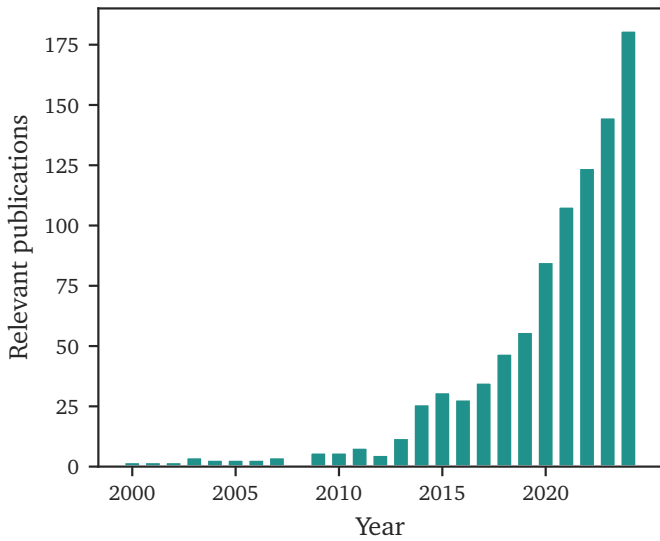


Figure 1: The number of publications on Scopus mentioning "lithium-ion battery" and "sensitivity analysis" in either title, abstract, or keywords over the past years, indicating a clear upwards trend.

Scheller et al. [24] use variance-based sensitivity analysis and a finite element all-solid-state battery model to determine key parameters critical for cell performance and their related optimization potential. Streb et al. [25] utilize variance-based sensitivity analysis to devise optimal experimental designs for the data-driven parametrization of a DFN model. Lin et al. [26] implement a framework for efficient variance-based sensitivity analysis and apply it to a three-dimensional lithium-ion battery model. R  ther et al. [27] use variance-based sensitivity analysis to investigate a numerical impedance model. Ko et al. [28] employ variance-based sensitivity analysis to determine the most relevant parameters serving as battery aging indicators, with subsequent parameter identification at different states of health. Chen et al. [29] use variance-based sensitivity analysis to find operating conditions that increase the sensitivity of specific parameters in an electrochemical-thermal battery model. While global sensitivity analysis is adequate for nonlinear models, the main drawback of the above works is that commonly available global sensitivity analysis approaches can only deal with scalar-valued quantities of interest. For time-dependent quantities, like the terminal voltage of a battery during charging or discharging, it is therefore necessary to resort to integrals over time, averages, or the selection of a single point in time. This is disadvantageous because integrating or averaging the quantity of interest over time might lead to a loss of information, and only selecting one or multiple points in time does not yield a comprehensive picture.

In order to alleviate the issue of arbitrarily producing a scalar value from a vectorial simulation result for sensitivity analysis, this work therefore implements an innovative framework for global sensitivity analysis of time-dependent

quantities of interest and applies it to the voltage response of the DFN model for a drive cycle with high dynamics. To the best of our knowledge, this is the first time parametric sensitivity is determined over a dynamic battery model output in a statistically rigorous fashion. This marks a significant leap in methodology and can aid future simulative battery research in dealing with research questions related to parametric sensitivity more robustly. Our particular contributions are the following:

- We reiterate the arguments from literature calling for alternatives to the OAT method in the case of nonlinear battery models (Section 2.1.1)
- We summarize the theoretical background of the novel sensitivity analysis methodology devised by Alexanderian et al. [30] (Section 2.1.3) and provide the open-source implementation used in this work.
- By leveraging the LiionDB [31], we show the wide spread of battery model parameters found in the literature, even in the case of identical electrode materials, which hinders parametrization from literature-derived values (Fig. 5).
- Using the aforementioned framework, we conduct a time-dependent global sensitivity analysis of the DFN model for a drive cycle (Section 4.1) and a subgroup analysis (Section 4.2) over the previously determined parameter range. In contrast to previous works, our study aggregates the parametric effects over the whole time-dependent trajectory and allows for a separation of first- and total-order effects.
- Furthermore, we investigate the model error when setting an increasing number of insensitive parameters to arbitrary values from literature (Section 4.3) as a guidance for battery modelling practitioners, given the widespread reliance on literature-based parameter values.

2. Background

2.1. Sensitivity analysis

The field of sensitivity analysis deals with the question of how to obtain a relative importance ranking of the parameters of a mathematical model. In this context, simulators are often seen as black-box functions of the general form

$$Y = f(\xi), \quad \xi \in \mathbb{R}^d, \quad (1)$$

where ξ is a d -dimensional vector of uncertain model parameters and Y is the corresponding model output. Elucidating the relationship between ξ and Y can be very challenging when f is a complex model.

Methods for sensitivity analysis are categorized into local and global approaches [32]. While local sensitivity analysis investigates the sensitivity around a single point in parameter space, global sensitivity analysis aims at providing a full picture across the whole parameter space.

2.1.1. The inadequacy of one-at-a-time methods

The OAT method is based on the idea of coarsely approximating the gradient of the response surface of a model around a reference point in parameter space in a finite difference fashion [32]. This is generally achieved by spanning a parameter space with minimum and maximum values for each considered parameter and then varying each parameter separately around its nominal value. By design, this approach cannot account for interactions of parameter combinations, since multiple parameters are never varied concomitantly.

The much bigger concern according to Saltelli et al. [7], however, is that the OAT method leaves the defined parameter space vastly underexplored. Varying parameters individually around their nominal value limits the exploration of the parameter space to a ‘‘hypercross’’ structure. In high-dimensional parameter spaces, this hypercross has neglectable coverage when compared to the entire volume of the space. This problem is illustrated well by imagining the enveloping hypersphere of the hypercross (Fig. 2) and computing volume ratios between the sphere and the entire parameter space. In 10 dimensions, one would obtain a volume ratio of $2.5 \cdot 10^{-3}$, which is a very generous upper bound estimate considering the hypercross constitutes only a very small fraction of the enveloping hypersphere. Therefore, the OAT approach leaves most of the parameter space unexplored for higher dimensional problems. For the sake of clarity, we complement these theoretical considerations with an illustrative example from literature in Appendix C.

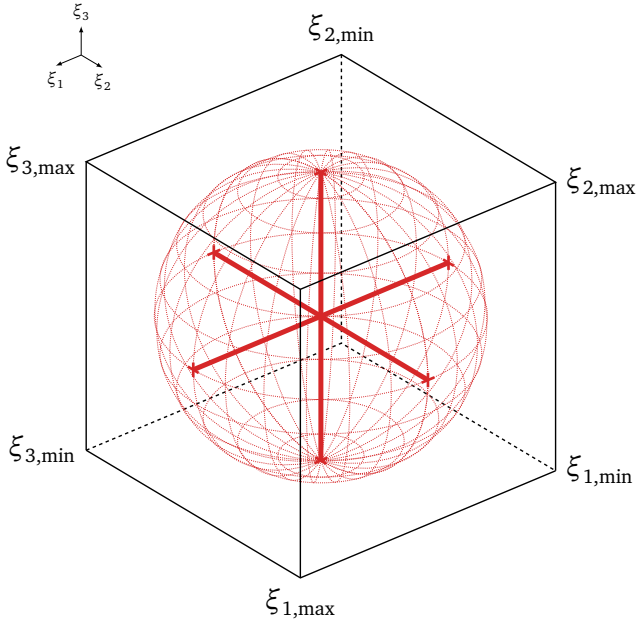


Figure 2: Visualization of a parameter space spanned by the three parameters ξ_1 , ξ_2 , and ξ_3 . The hypercross structure sampled by OAT methods and its enveloping hypersphere inhabit only a fraction of the entire volume. This fraction decreases very rapidly as the number of parameters increases [7].

Due to these limitations, OAT methods are considered unsuitable for nonlinear models [7, 8, 33]. Their simplicity and ease of use make them a widely employed choice regardless, especially in battery research.

2.1.2. Variance-based sensitivity analysis

Variance-based sensitivity analysis tries to apportion the variance of the model response to each individual parameter, thereby providing a measure of the parameter’s importance. This is facilitated by the Hoeffding-Sobol’ decomposition of f , which is a sum of functions of increasing dimension [34, 35]

$$f(\xi) = f_0 + \sum_{i=1}^d f_i(\xi_i) + \sum_{i<j}^d f_{ij}(\xi_j, \xi_i) + \dots + f_{1,2,\dots,d}(\xi_1, \xi_2, \dots, \xi_d), \quad (2)$$

where f_0 is a constant, the f_i are one-dimensional functions depending only on the i -th component of ξ , $f_{i,j}$ are two-dimensional functions depending on the i -th and j -th component, etc. If we now consider ξ a random vector

$$\xi = \{\xi_1, \dots, \xi_d\}, \quad \text{with } \xi_i \sim \mathcal{P}_i, \quad i \in \{1, \dots, d\}, \quad (3)$$

where each component ξ_i is a random variable distributed according to its probability distribution \mathcal{P}_i , the model output $Y = f(\xi)$ becomes a random variable [36]. Using (2), the total variance of the output $D = \mathbb{V}[Y]$ can similarly be decomposed into partial variances [37]

$$D = \sum_i^d D_i + \sum_{i<j}^d D_{ij} + \dots + D_{1,2,\dots,d}, \quad (4)$$

which, upon dividing by D , yields the Sobol’ indices of all orders

$$1 = \sum_i^d S_i + \sum_{i<j}^d S_{ij} + \dots + S_{1,2,\dots,d}. \quad (5)$$

The S_i are called *first-order* or *main effect* Sobol’ indices, as they relate the variance caused solely by individual parameters to the total variance. The *total-order* or *total effect* Sobol’ indices S_i^{tot} represent the effect of a parameter when taking all possible higher-order interactions with other parameters into account. They are defined as [36]

$$S_i^{\text{tot}} = \frac{\sum_{k \in \mathcal{X}_i} D_k}{D} = \frac{D_i + D_{ij} + \dots + D_{1,\dots,i,\dots,d}}{D}, \quad (6)$$

where \mathcal{X}_i is an index set containing all combinations that include i . The expression in (6) is equivalent to the sum of all Sobol’ indices that consider the i -th parameter. Sobol’ indices therefore provide a sensitivity measure by quantifying the proportion of the total uncertainty that is caused by each individual input parameter of the model.

2.1.3. Extension to time-dependent quantities of interest

In the above derivation, the model response Y was considered a scalar. Alexanderian et al. [30] introduced novel approaches for conducting variance-based sensitivity analyses

for time-dependent model outputs, which will be summarized here. In the following, we will consider a time-dependent model

$$Y = f(t, \xi), \quad t \in [0, T]. \quad (7)$$

While it was previously possible to compute Sobol' indices or other global sensitivity metrics for each point in time t_k of a grid

$$\{t_k\}_{k=1}^{N_{\text{quad}}} \quad \text{with} \quad t_{k-1} < t_k \quad \text{and} \quad t_1 = 0, \quad t_{N_{\text{quad}}} = T, \quad (8)$$

as done by, e.g., Hadigol et al. [38] or Constantine and Doostan [39], this approach presents two major shortcomings. Firstly, since models in science and engineering are generally heteroscedastic, i.e., their variance is not constant over time, the relative importance of parameters over time is inconclusive, as parameters contributing heavily to a comparably small variance should be overall considered less important. Secondly, the temporal correlation structure of the model response is neglected, because each $f(t_k, \xi)$ is treated independently.

For the aforementioned reasons, Alexanderian et al. [30] devised algorithms based on surrogate models and spectral representations that alleviate both issues and will be outlined in the following. The underlying idea is the generalization of the previously defined classical Sobol' indices

$$S_i = \frac{D_i}{D}, \quad S_i^{\text{tot}} = \frac{\sum_{k \in \mathcal{X}_i} D_k}{D} \quad (9)$$

to time-dependent variances

$$\mathfrak{S}_i(T) = \frac{\int_0^T D_i(t) dt}{\int_0^T D(t) dt}, \quad \mathfrak{S}_i^{\text{tot}}(T) = \frac{\int_0^T \sum_{k \in \mathcal{X}_i} D_k(t) dt}{\int_0^T D(t) dt}. \quad (10)$$

By employing a quadrature rule with nodes and weights $\{t_m, w_m\}_{m=1}^{N_{\text{quad}}}$ on the interval $[0, T]$, we can solve the integrals in (10) numerically via

$$\begin{aligned} \mathfrak{S}_i(T) &\approx \frac{\sum_{m=1}^{N_{\text{quad}}} w_m D_i(t_m)}{\sum_{m=1}^{N_{\text{quad}}} w_m D(t_m)}, \\ \mathfrak{S}_i^{\text{tot}}(T) &\approx \frac{\sum_{m=1}^{N_{\text{quad}}} \sum_{k \in \mathcal{X}_i} w_m D_k(t_m)}{\sum_{m=1}^{N_{\text{quad}}} w_m D(t_m)}. \end{aligned} \quad (11)$$

By constructing pointwise-in-time polynomial chaos (PC) surrogate models, one can obtain the partial variances $D_i(t_m)$ and $D_k(t_m)$. A PC expansion is generally of the form

$$f(t, \xi) = \sum_{k=1}^{\infty} c_k(t) \Psi_k(\xi) \approx \sum_{k=1}^{N_{\text{PC}}} c_k(t) \Psi_k(\xi), \quad (12)$$

where $\{\Psi_k\}_{k=1}^{N_{\text{PC}}}$ is a set of orthogonal polynomials or an orthonormal polynomial basis, the $\{c_k\}_{k=1}^{N_{\text{PC}}}$ are expansion coefficients and N_{PC} is the finite number of terms the exact PC expansion is truncated to. Since ξ is a d -dimensional random vector, the Ψ_k are d -variate polynomials. The benefit of PC

expansion-based surrogate models lies in their ability to provide analytical expressions for the partial variances [36]. This enables us to rewrite (11) as

$$\begin{aligned} \mathfrak{S}_i(T) &\approx \frac{\sum_{m=1}^{N_{\text{quad}}} \sum_{k \in \mathcal{J}_i} \|\Psi_k\|^2 w_m c_k(t_m)^2}{\sum_{m=1}^{N_{\text{quad}}} \sum_{k=1}^{N_{\text{PC}}} \|\Psi_k\|^2 w_m c_k(t_m)^2}, \\ \mathfrak{S}_i^{\text{tot}}(T) &\approx \frac{\sum_{m=1}^{N_{\text{quad}}} \sum_{k \in \mathcal{X}_i} \|\Psi_k\|^2 w_m c_k(t_m)^2}{\sum_{m=1}^{N_{\text{quad}}} \sum_{k=1}^{N_{\text{PC}}} \|\Psi_k\|^2 w_m c_k(t_m)^2}, \end{aligned} \quad (13)$$

where \mathcal{J}_i is an index set that includes all terms in the PC expansion that consider only the i -th parameter. If the Ψ_k form an orthonormal basis, then $\|\Psi_k\|^2 = 1 \forall k$.

The second approach from Alexanderian et al. [30] for computing the generalized Sobol' indices relies on spectral representations, namely Karhunen-Loève (KL) expansions. The KL expansions are of the form

$$f(t, \xi) = f_0 + \sum_{i=1}^{\infty} f_i(\xi) e_i(t) \approx f_0 + \sum_{i=1}^{N_{\text{KL}}} f_i(\xi) e_i(t), \quad (14)$$

with f_0 being the mean of the time-dependent process $\mathbb{E}[f(t, \xi)]$, the $f_i(\xi)$'s are expansion coefficients with variance $\mathbb{V}[f_i(\xi)] = \lambda_i$, and λ_i and e_i are the eigenvalues and eigenvectors of the covariance operator of $f(t, \xi)$.

To construct a KL expansion, $f(t, \xi)$ needs to be a centered process, i.e., it needs to have zero mean. The first step is therefore to center the process by subtracting the mean from all N model evaluations $\{f(t_m, \xi^j)\}_{j=1}^N$ at each point in time t_m

$$f_c(t_m, \xi^k) = f(t_m, \xi^k) - \frac{1}{N} \sum_{j=1}^N f(t_m, \xi^j), \quad (15)$$

with $k \in \{1, \dots, N\}$ and $m \in \{1, \dots, N_{\text{quad}}\}$.

Then, we can construct the covariance matrix \mathbf{K} of the centered function evaluations by obtaining its elements K_{lm} via

$$K_{lm} = \frac{1}{N-1} \sum_{k=1}^N f_c(t_l, \xi^k) f_c(t_m, \xi^k), \quad (16)$$

with $l, m \in \{1, \dots, N_{\text{quad}}\}$.

The solution of the eigenvalue problem

$$\mathbf{W}^{\frac{1}{2}} \mathbf{K} \mathbf{W}^{\frac{1}{2}} \mathbf{u}_i = \lambda_i \mathbf{u}_i, \quad (17)$$

with $\mathbf{W} = \text{diag}(w_1, w_2, \dots, w_{N_{\text{quad}}})$, $i \in \{1, \dots, N_{\text{quad}}\}$,

specifically the spectral decay of the eigenvalues λ_i , which informs the truncation level N_{KL} , lies at the heart of this approach. The truncation level should be chosen such that the fraction of the total variance captured by the truncated KL expansion, given as

$$r_{N_{\text{KL}}} = \frac{\sum_{i=1}^{N_{\text{KL}}} \lambda_i}{\sum_{i=1}^{\infty} \lambda_i}, \quad (18)$$

is sufficiently large. If one can obtain a large fraction $r_{N_{\text{KL}}}$ with a small truncation level N_{KL} , the respective process is

deemed a *low-rank* process. This means that almost all the uncertainty in f is quantified by the N_{KL} KL modes.

To compute the KL modes, we first need to obtain the eigenvectors e_i from u_i via

$$e_i = W^{-\frac{1}{2}} u_i, \quad i \in \{1, \dots, N_{\text{quad}}\}. \quad (19)$$

We can then compute

$$f_i(\xi^k) = \sum_{m=1}^{N_{\text{quad}}} w_m f_c(t_m, \xi^k) e_i^m, \quad (20)$$

with $i \in \{1, \dots, N_{\text{KL}}\}$ and $k \in \{1, \dots, N\}$. This leaves us with N realizations $f_i(\xi^k)$ of each mode f_i , which we can use to construct a PC surrogate model for each mode

$$f_i(\xi) \approx \sum_{k=1}^{N_{\text{PC}}} c_k^i \Psi_k(\xi). \quad (21)$$

Using these PC expansions, we can again efficiently compute the generalized Sobol' indices as

$$\begin{aligned} \mathfrak{S}_i(T) &\approx \frac{\sum_{i=1}^{N_{\text{KL}}} \sum_{k \in \mathcal{J}_i} \|\Psi_k\|^2 (c_k^i)^2}{\sum_{k=1}^{N_{\text{KL}}} \lambda_i}, \\ \mathfrak{S}_i^{\text{tot}}(T) &\approx \frac{\sum_{i=1}^{N_{\text{KL}}} \sum_{k \in \mathcal{X}_i} \|\Psi_k\|^2 (c_k^i)^2}{\sum_{k=1}^{N_{\text{KL}}} \lambda_i}. \end{aligned} \quad (22)$$

In the following, we will refer to the approaches defined by equation (13) and equation (22) as PC method and KL method respectively. Please note that while both methods employ PC expansions, the PC method explicitly refers to the use of pointwise-in-time PC surrogate models. Fig. 3 shortly summarizes the main differences between the two methods. It should be noted that for the analysis, all model outputs need to span the same time interval, which limits its applicability in cases where the simulated duration varies between runs or depends on the input parameters. This could be the case in (dis-)charge simulations with a constant current, when the sampled parameters lead to varying battery capacities.

2.2. The Doyle-Fuller-Newman model

The DFN or p2D model was devised by Doyle, Fuller, and Newman [5, 6] in the early 1990s and has since become an invaluable tool in battery research. It is based on porous electrode theory and Butler-Volmer kinetics to describe the relevant battery processes on the continuum scale. To this end, the cell model is divided into a positive electrode, separator, and negative electrode domain. Each of these domains is thought of as a porous medium filled with electrolyte, and the particles in the electrode domains are considered perfectly spherical. This porous medium, however, is not fully resolved but rather homogenized and projected onto the x -dimension. The spherical particles are placed along this one-dimensional axis in the positive and negative electrode domains to act as representative electrode particles (Fig. 4). The diffusion of

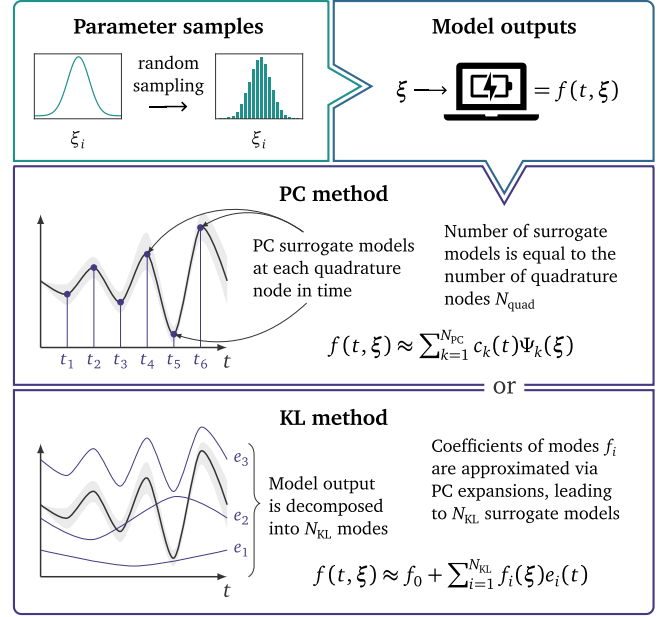


Figure 3: A visual summary of the main differences between the PC method and the KL method.

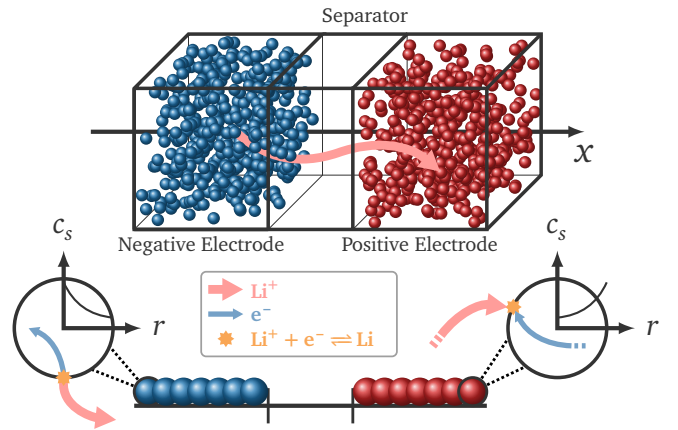


Figure 4: Schematic depiction of the DFN model during discharge.

lithium inside the solid part of the electrode is resolved over the particle's radius.

The constituting equations of the DFN model can be split into three distinct groups, namely equations that describe charge conservation, mass conservation, and electrochemical kinetics. In the following, we closely adhere to the conventions of Sulzer et al. [40, 41]. Since the model describes a lithium-ion cell, the number of transferred electrons is $z = 1$ and all involved ions are singly charged.

Charge conservation: The spatial gradient of the current in the electrolyte i_1 is zero in the separator, but equal to the intercalation current in the electrode domains

$$\frac{\partial i_{1,k}}{\partial x} = \begin{cases} a_k j_k, & k \in \{\text{neg, pos}\} \\ 0, & k = \text{sep}, \end{cases} \quad (23)$$

where a is the specific surface area and j the intercalation current density. The index $k \in \{\text{neg, sep, pos}\}$ describes the domain on which the equations hold, with neg denoting the negative electrode domain, sep the separator domain, and pos the positive electrode domain. The current in the electrolyte itself can be obtained via

$$i_{1,k} = \varepsilon_k^{b_k} \kappa \left(-\frac{\partial \phi_{1,k}}{\partial x} + 2\Theta(1-t^+) \frac{RT}{F} \frac{\partial \ln c_{1,k}}{\partial x} \right), \quad (24)$$

$$k \in \{\text{neg, sep, pos}\},$$

where ε is the porosity, b the Bruggeman coefficient, ϕ_1 is the potential in the liquid phase, t^+ is the transference number of the lithium ions, R is the universal gas constant, F the Faraday constant, T is the temperature, c_1 is the concentration of lithium ions in the electrolyte, and $\Theta := 1 + \frac{\partial \ln f}{\partial \ln c_1}$ is the so-called *thermodynamic factor*, which is treated as a parameter. It also holds that

$$I - i_{1,k} = -\sigma_k \frac{\partial \phi_{s,k}}{\partial x}, \quad k \in \{\text{neg, pos}\}, \quad (25)$$

where I is the total applied current density, σ is the electric conductivity, and ϕ_s is the potential in the solid phase. Since there is no current flowing through the solid phase in the separator, we have $I - i_{1,\text{sep}} = 0$.

Mass conservation: The change in lithium ion concentration in the electrolyte c_1 over time is given by

$$\varepsilon_k \frac{\partial c_{1,k}}{\partial t} = -\frac{\partial N_{1,k}}{\partial x} + \frac{1}{F} \frac{\partial i_{1,k}}{\partial x}, \quad k \in \{\text{neg, sep, pos}\} \quad (26)$$

with the molar flux in the liquid phase N_1 defined as

$$N_{1,k} = -\varepsilon_k^{b_k} D_1 \frac{\partial c_{1,k}}{\partial x} + \frac{t^+}{F} i_{1,k}, \quad k \in \{\text{neg, sep, pos}\}, \quad (27)$$

where D_1 is the diffusion coefficient of the liquid phase. Lithium ion transport in the solid phase is described by Fickian diffusion

$$\frac{\partial c_{s,k}}{\partial t} = -\frac{1}{r_k^2} \frac{\partial}{\partial r_k} (r_k^2 N_{s,k}), \quad k \in \{\text{neg, pos}\}, \quad (28)$$

where c_s is the concentration of lithium in the solid phase, r denotes the radial coordinate of the spherical electrode particle, and the molar flux in the solid phase N_s is

$$N_{s,k} = -D_{s,k} \frac{\partial c_{s,k}}{\partial r_k}, \quad k \in \{\text{neg, pos}\}, \quad (29)$$

with D_s being the diffusion coefficient of the solid phase.

Electrochemical kinetics: The electrode current density j is given by the Butler-Volmer equation

$$j_k = j_{0,k} \left(\exp\left(\frac{F\alpha_{\text{ox}}}{RT} \eta_k\right) - \exp\left(-\frac{F\alpha_{\text{red}}}{RT} \eta_k\right) \right), \quad (30)$$

$$k \in \{\text{neg, pos}\},$$

where $\alpha_{\text{ox}} = \alpha_{\text{red}} = 0.5$ are the charge transfer coefficients of the oxidation and reduction reaction respectively, η stands for the overpotential, and j_0 is the exchange current density, computed as

$$j_{0,k} = F k_0 c_{s,k}^{\alpha_{\text{red}}} (1 - c_{s,k})^{\alpha_{\text{ox}}} c_{1,k}^{\alpha_{\text{ox}}} \Big|_{r_k=R_k}, \quad k \in \{\text{neg, pos}\}, \quad (31)$$

with k_0 as the reaction rate constant and R_k being the particle radius. Note that different conventions exist regarding the form of equation (31), warranting careful consideration of the units of the reaction rate constant. The overpotential is defined as

$$\eta_k = \phi_{s,k} - \phi_{1,k} - U_{0,k}(c_{s,k}|_{r_k=R_k}), \quad k \in \{\text{neg, pos}\}, \quad (32)$$

where ϕ_s is the potential in the solid phase and U_0 is the equilibrium potential, also known as open-circuit potential or open-circuit voltage (OCV), which depends on the surface concentration of the electrode particles.

Boundary and initial conditions: On the left and right boundary of the domain, no current flows out of the electrolyte, i.e.,

$$i_{1,\text{neg}}|_{x=0} = 0 \quad \text{and} \quad i_{1,\text{pos}}|_{x=L} = 0, \quad (33)$$

where $L = L_{\text{neg}} + L_{\text{sep}} + L_{\text{pos}}$ is the sum of the length of each domain.

On the interface of negative electrode and separator, the potentials in the liquid phase are equal

$$\phi_{1,\text{neg}}|_{x=L_{\text{neg}}} = \phi_{1,\text{sep}}|_{x=L_{\text{neg}}} \quad (34)$$

and the currents are equal to the applied current

$$i_{1,\text{neg}}|_{x=L_{\text{neg}}} = i_{1,\text{sep}}|_{x=L_{\text{neg}}} = I. \quad (35)$$

The same holds for the interface of the separator and the positive electrode

$$\phi_{1,\text{sep}}|_{x=L-L_{\text{pos}}} = \phi_{1,\text{pos}}|_{x=L-L_{\text{pos}}} \quad \text{and} \quad (36)$$

$$i_{1,\text{sep}}|_{x=L-L_{\text{pos}}} = i_{1,\text{pos}}|_{x=L-L_{\text{pos}}} = I.$$

Akin to the currents, the molar fluxes in the electrolyte phase are zero at the left and right boundaries, i.e.,

$$N_{1,\text{neg}}|_{x=0} = 0, \quad N_{1,\text{pos}}|_{x=L} = 0. \quad (37)$$

And similarly, at both interfaces of the electrodes and the separator the concentrations in the liquid phase and the molar fluxes are equal, which means that at the interface of the negative electrode

$$\begin{aligned} c_{l,\text{neg}}|_{x=L_{\text{neg}}} &= c_{l,\text{sep}}|_{x=L_{\text{neg}}} \quad \text{and} \\ N_{l,\text{neg}}|_{x=L_{\text{neg}}} &= N_{l,\text{sep}}|_{x=L_{\text{neg}}}, \end{aligned} \quad (38)$$

and at the interface of the positive electrode we have

$$\begin{aligned} c_{l,\text{sep}}|_{x=L-L_{\text{pos}}} &= c_{l,\text{pos}}|_{x=L-L_{\text{pos}}} \quad \text{and} \\ N_{l,\text{sep}}|_{x=L-L_{\text{pos}}} &= N_{l,\text{pos}}|_{x=L-L_{\text{pos}}}. \end{aligned} \quad (39)$$

Inside the electrode particles, a zero Dirichlet condition is enforced at the center of the particle for the molar flux

$$N_{s,k}|_{r_k=0} = 0, \quad k \in \{\text{neg}, \text{pos}\}, \quad (40)$$

while at the particle surface, the molar flux depends on the faradaic current density, such that

$$N_{s,k}|_{r_k=R_k} = \frac{j_k}{F}, \quad k \in \{\text{neg}, \text{pos}\}. \quad (41)$$

Finally, we set initial values as initial conditions for the concentrations in the liquid and solid phases, i.e.,

$$\begin{aligned} c_{s,k}(x, r, t = 0) &= c_{s,k,0}, \quad k \in \{\text{neg}, \text{pos}\} \quad \text{and} \\ c_{l,k}(x, t = 0) &= c_{l,k,0}, \quad k \in \{\text{neg}, \text{sep}, \text{pos}\}. \end{aligned} \quad (42)$$

In the following, the parameters of the model are considered scalars independent of state of charge or concentration. Since we consider the isothermal case and do not include a thermal model, the model parameters are also not dependent on temperature.

3. Methods

3.1. General

For the numerical treatment of the equations described in section 2.2, we rely on the DFN model implementation provided by the Python-based open-source framework PyBaMM [40]. We use PyBaMM v24.9.0. The base parametrization of our model is derived from the parameter set by Marquis et al. [42] for a Kokam SLPB78205130H cell. Since we sample uncertain parameter vectors, the base parametrization only provides values for the parameters not varied over the course of the sensitivity analysis, e.g., the OCV curves, the electrode area, etc. We employ the CasADi solver [43] and the default discretization, i.e., 20 mesh nodes in each subdomain in the x -dimension, as well as 20 mesh nodes in the r -dimension of each particle.

Since the parameter space is relatively vast, some randomly drawn parameter vectors might lead to convergence issues for the solver. We remedy this by omitting any parameter vectors that lead to non-converged simulations. This is well-justified because we utilize an independent and identically distributed random sampling approach and not quasi-random

samples or quadrature-based approaches [44]. The number of samples reported in section 4 pertains to the total number of simulation runs irrespective of convergence. However, the observed number of failed simulations does not exceed 0.003% for $N = 100000$, which is negligibly small.

We employ a composite trapezoidal rule as the numerical quadrature rule mentioned in section 2.1.3. All simulations and computations were conducted on a Fujitsu Celsius workstation with two Intel Xeon Gold 6128 CPUs and 128 GB of RAM. Shared-memory parallelization of our code is achieved using `joblib` [45]. Our Python implementation of the algorithms outlined in section 2.1.3 and used throughout this work is available on GitHub¹.

3.2. Implementational details

The approaches described in section 2.1.3 depend heavily on generalized PC surrogate models to either approximate the model response or the KL modes. As mentioned above, these PC expansions are exact in the limit of infinite terms, but need to be truncated for reasons of computational feasibility. The classical truncation scheme retains only polynomials with total degree up to some integer value p , such that $\|\alpha\|_1 \leq p$, where α is the vector of exponents of a multivariate polynomial in the expansion. We call p the *order* of the PC expansion and consider expansions truncated this way *full* expansions. Since this truncation scheme leads to $N_{\text{PC}} = \frac{(d+p)!}{d!p!}$ polynomials and corresponding coefficients, this ansatz quickly becomes impractical for high-dimensional problems with many uncertain parameters, at least for higher order PC expansions [36]. We therefore also explore the use of an alternative truncation scheme better suited for higher dimensional cases based on the q -quasi-norm, namely *hyperbolic cross truncation*, which specifies

$$\|\alpha\|_q \leq p, \quad \text{where} \quad \|\alpha\|_q := \left(\sum_{i=1}^d \alpha_i^q \right)^{\frac{1}{q}} \quad (43)$$

and thereby removes a lot of high-order interactions for $q \in (0, 1)$, while keeping main effects and low-order interactions in the expansion [46]. The rationale behind preferably eliminating high-order interactions lies in the *sparsity-of-effects principle* [47]. We refer to the resulting expansions as *sparse* PC expansions. We employ `chaospy` [48] for PC expansions and related probabilistic tools.

To determine the coefficients of the PC expansion and obtain a surrogate model, we use linear regression. Specifically, we utilize both ordinary least squares regression (OLS) and least angle regression (LARS) and compare their results in section 4. While OLS targets the titular *least squares problem*, i.e., the minimization of the squared residual, LARS aims at minimizing the L_1 norm. This makes LARS particularly suited for high-dimensional regression problems with limited data, especially since LARS is able to further sparsify the

¹Source code available from <https://github.com/ezonta/TDGS>

PC expansion by removing polynomials it deems irrelevant to the regression target. LARS achieves this by setting all coefficients to zero and increasing them one after another based on their correlation to the data. However, it also comes with the drawback of shrinkage on the coefficient estimates, which means that they are biased towards zero [49]. We rely on `scikit-learn` [50] for its implementation of both regression algorithms.

We observe that in some cases the eigenvalues obtained from the discretized covariance operator deviate from the total variance estimated by the PC surrogate model of the KL mode. Our implementation of the algorithm based on KL expansions therefore checks for a relative error smaller than 10% between the variance derived from the eigenvalues and the PC coefficients before computing the Sobol' indices. If the error exceeds this bound, the sum of PC variances is used instead of the sum of dominant eigenvalues in the denominator of (22). The mismatch does not seem to stem from an insufficiently sampled covariance matrix and the adjustment produces Sobol' indices in good agreement with those obtained via (13). The cause of this divergence will have to be investigated further.

3.3. Study design

3.3.1. Considered parameters and parameter ranges

In the present study, we consider 24 parameters of the DFN model, namely the maximum solid phase concentration c_s^{\max} , reaction rate constant k_0 , electrical conductivity σ , solid phase diffusivity D_s , and particle radius R of the positive and negative electrode; the layer thickness L , porosity ε_l , and Bruggemann coefficient b of the positive electrode, separator, and negative electrode; as well as the thermodynamic factor Θ , liquid phase diffusivity D_l , initial electrolyte concentration $c_{l,0}$, ionic conductivity of the electrolyte κ , and the transference number t^+ .

In order to obtain sensible parameter ranges that reflect the actual prevalence in battery modeling research, we utilized the `LiionDB` database devised by Wang et al. [15]. The `LiionDB` collects battery model parameters reported in the literature. We queried the database for data from lithium nickel manganese cobalt oxide (NMC) positive electrodes regardless of composition, graphite negative electrodes, and LiPF_6 -based electrolytes. We took into account all available data points at different temperatures, states of charge, etc., to further generalize the intervals. There was no data available in the database for $c_{l,0}$, which is why we resorted to basing its range off of values from literature [9, 11, 15, 51, 52]. The validity of negative transference numbers is debated [53, 54]. Nevertheless, we opted to keep the obtained intervals from the `LiionDB` unchanged. The parameter ranges used in this work and ranges from comparable studies are shown in Fig. 5. Numerical values can be found in Tab. A.2.

The electrode area A is kept constant throughout the study to get consistent current densities. We do not sample the solid volume fraction ε_s , as it would be dependent on ε_l , which would break the independency assumption of the methodology and would require more sophisticated treatment [55].

For reasons of simplicity, we set $\varepsilon_s = 1 - \varepsilon_l$ and do not account for an inactive material volume fraction, as we do not suspect its influence to extend beyond the caused change in cell capacity. As is typical for sensitivity analyses, we sample scalar parameters and do not consider dependence of parameters on state of charge or concentration, because sampling functional parameters requires significantly more effort [56]. We also do not sample the initial solid concentration $c_{s,0}$ for each electrode, but rather set it to $\frac{1}{2}c_s^{\max}$, such that the initial voltage is the same for every sampled parameter vector, because

$$U(t=0) = U_{0,\text{pos}} \left(\frac{c_{s,0,\text{pos}}}{c_{s,\text{pos}}^{\max}} \right) - U_{0,\text{neg}} \left(\frac{c_{s,0,\text{neg}}}{c_{s,\text{neg}}^{\max}} \right). \quad (44)$$

This of course leads to a randomized cell balancing, which will be addressed in section 3.3.2.

3.3.2. Current profiles

Since each sampled parameter vector will lead to a different cell capacity, the applied current profile will have to be appropriate for the whole range of resulting capacities. The actual capacity, however, can not easily be obtained from the sampled parameter values, due to the randomized balancing. This means that we need some estimate for the cell capacity and that we ought to tailor our current magnitude such that we do not exceed too large C-rates in the low capacity samples, which might lead to convergence issues. To that end, we compute the theoretical limiting areal capacity C_{theo} of each parameter vector

$$C_{\text{theo}} = \min(C_{\text{theo,neg}}, C_{\text{theo,pos}}), \quad (45)$$

where

$$C_{\text{theo},k} = F \cdot c_{s,k}^{\max} \cdot L_k \cdot \varepsilon_{l,k}, \quad k \in \{\text{neg}, \text{pos}\}. \quad (46)$$

As C_{theo} is an estimate of the cell capacity neglecting electrode utilization determined by the cell balancing, it admits a theoretical C_{theo} -rate by dividing the applied current density through C_{theo} . This C_{theo} -rate is a lower bound estimate of the actual C-rate, coinciding in the case of full utilization of the limiting electrode, and will be used in the following to contrive the current magnitudes of the applied current profiles. In the case of underutilization of the limiting electrode in the considered voltage range, the actual C-rate will be higher than the C_{theo} -rate.

We investigate the simulation of a highly dynamic current profile in this study, namely a scaled version of the US06 drive cycle, delivered with `PyBaMM` up until v24.1. The scaling is chosen such that the peak C_{theo} -rate does not exceed 2 h^{-1} . We could arguably have chosen a larger scaling factor at the expense of a potentially higher number of non-converged simulations, but the error investigation for the unscaled drive cycle seems to suggest that the results can to some extent be generalized for different scaling factors (Section 4.3). Fig. 6 visualizes and summarizes our deliberations on the relationship of theoretical limiting capacity and current magnitude for the load profile. The large variation in N/P-ratios (Fig. 6b)

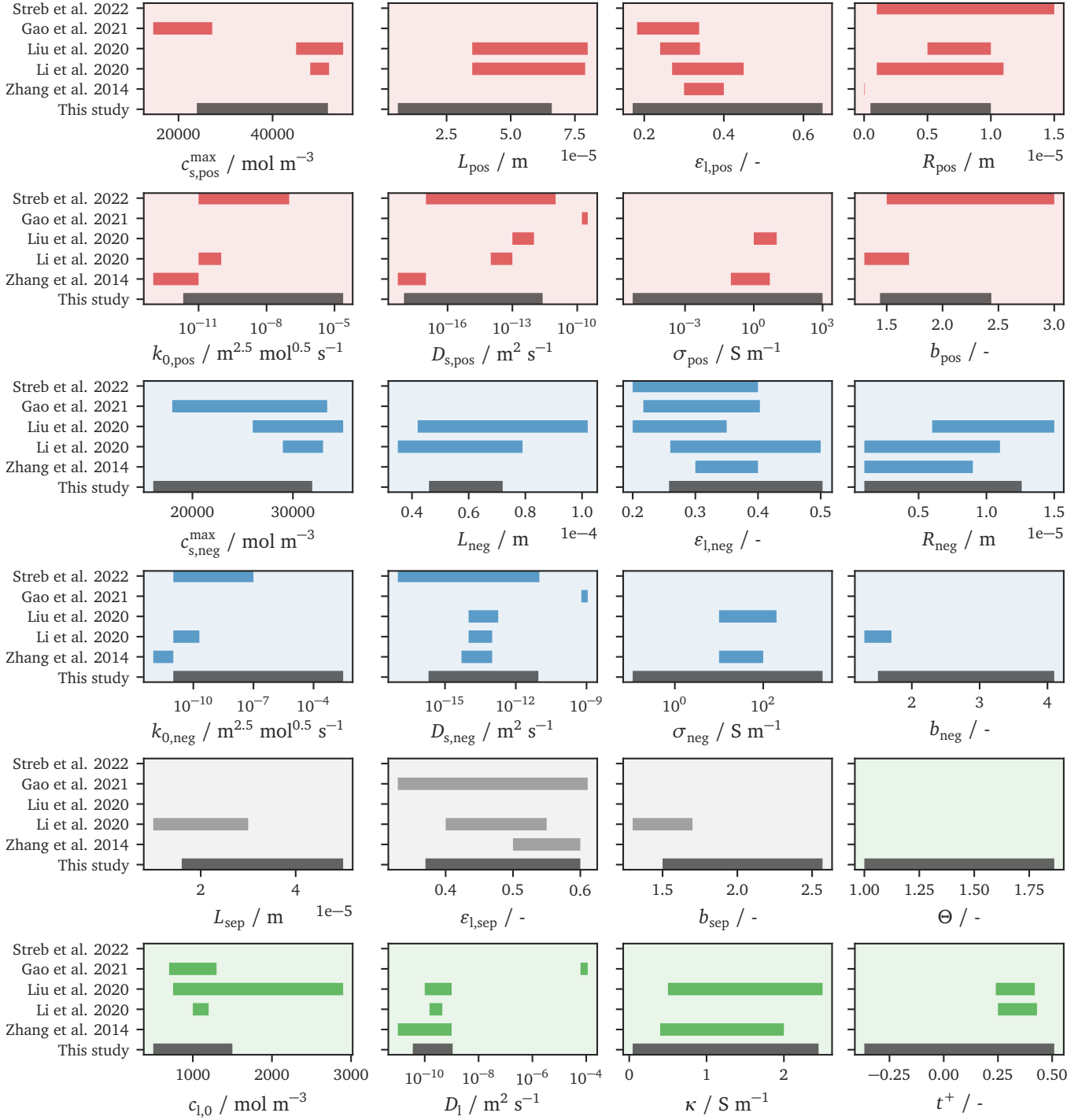


Figure 5: An overview of the parameter ranges covered in this study and in similar works by Zhang et al. [14], Li et al. [11], Liu et al. [12], Gao et al. [52], and Streb et al. [25]. The parameter ranges obtained from the LiionDB agree well with most of the literature ranges, albeit with a tendency of being more extensive. However, some parameter intervals are smaller than their counterparts from literature. For L_{neg} , this can be explained by the availability of only two data points. The discrepancy between our value range for $c_{1,0}$ and the interval of Liu et al. is relativized by the fact that various literature sources were utilized to construct the range. The obtained interval for t^+ extends into the negative numbers, which is not considered in any of the selected literature.

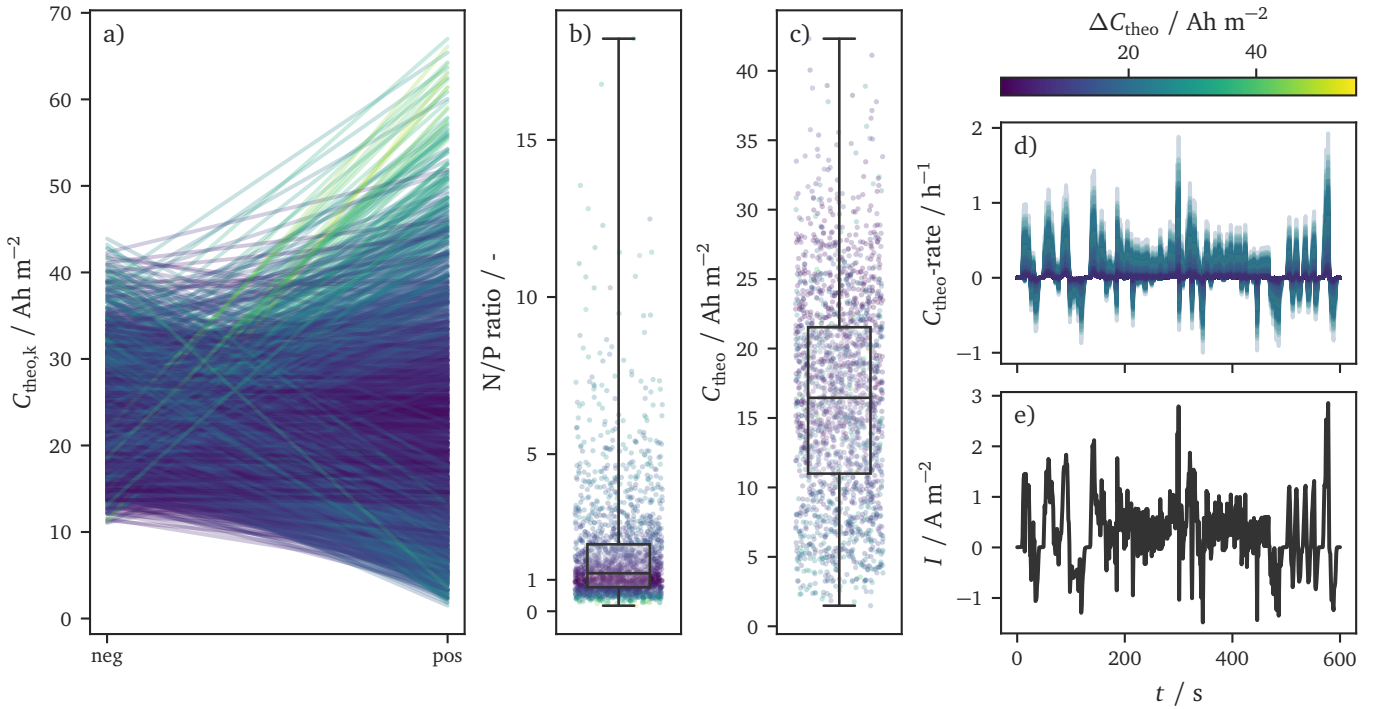


Figure 6: Visualization of the theoretical capacity of 2000 representative parameter samples to outline the scaling procedure for the drive cycle load profile. a) The balancing of the parameter samples depicted as a spaghetti plot connecting the theoretical capacity of the negative electrode with the theoretical capacity of the positive electrode. b) The resulting N/P ratio, i.e., the ratio of the capacity of the negative electrode over the capacity of the positive electrode. We can see that the median value is slightly larger than one, which agrees well with typical cells. c) A scatter plot of the limiting theoretical capacity, which corresponds to the minimum of each line in the spaghetti plot. In around 60% of cases, the positive electrode is the limiting one. Since the spread is quite wide, the current magnitude of the drive cycle needs to be scaled, such that most simulations converge. In case of full utilization of the limiting electrode, the theoretical limiting capacity is the capacity of the cell. The scaled drive cycle is presented as d) the theoretical C-rates related to the theoretical limiting capacities and e) as a current density. The color of the lines and dots indicates the absolute difference in electrode capacity.

indicates that the depth of discharge will vary significantly between samples, making it difficult to draw conclusions with regard to the influence of the state of charge.

3.3.3. Subgroup analysis

We additionally perform a subgroup sensitivity analysis, aiming at a better resolved picture of the overall parametric sensitivity by decoupling high and low sensitivity scales. The grouping separates the parameters into parameters related to the negative electrode, positive electrode, separator, and electrolyte. In the negative and positive electrodes, the parameters are further subdivided into capacity-related and non-capacity-related parameters. This yields six groups in total, which are shown in Tab. 1. The capacity-related parameters of the positive and negative electrode are found in group 1 and 3 respectively and the non-capacity-related parameters of each electrode in group 2 and 4 correspondingly. The parameters related to the separator are in group 5 and the electrolyte-related parameters comprise group 6.

In order to still obtain a sufficient exploration of parameter space in the subgroup analysis, we vary the fixed out-of-group parameters over a space-filling design of 30 points obtained from Latin hypercube sampling (LHS) over the whole pa-

Table 1: Parameter groupings for the subgroup sensitivity analysis based on domain affiliation.

Group	Parameters
1	$c_{s, \text{pos}}^{\text{max}}, L_{\text{pos}}, \epsilon_{l, \text{pos}}$
2	$b_{\text{pos}}, k_{0, \text{pos}}, \sigma_{\text{pos}}, D_{s, \text{pos}}, R_{\text{pos}}$
3	$c_{s, \text{neg}}^{\text{max}}, L_{\text{neg}}, \epsilon_{l, \text{neg}}$
4	$b_{\text{neg}}, k_{0, \text{neg}}, \sigma_{\text{neg}}, D_{s, \text{neg}}, R_{\text{neg}}$
5	$L_{\text{sep}}, \epsilon_{l, \text{sep}}, b_{\text{sep}}$
6	$\Theta, c_{1,0}, D_1, \kappa, t^+$

parameter space. LHS attempts to cover the whole parameter space by sampling from a partition of equiprobable hypercubes, thereby stratifying the probability distribution [57]. We average the obtained Sobol' indices of each group over all these individual sensitivity analyses for different out-of-group parameter values.

4. Results and discussion

We would like to preface this section with a short consideration: While the purely mathematical interpretation of Sobol'

indices is rather straightforward, ascribing the sensitivity to some underlying physical processes described by the model is not as trivial and requires substantial domain knowledge. The matter is further complicated by the influence of the parameter ranges and current profile on the analysis. A *general* sensitivity analysis, in the sense that it assesses the parametric sensitivity of the DFN model regardless of use case is therefore unfeasible. In the following, we aim to provide a discussion on general takeaways both methodologically and with regard to the DFN model, with the latter tending to be a bit more speculative, since sensitivity analysis does not provide any evidence on the underlying model behavior.

4.1. Full analysis

Fig. 7 shows the voltage response over time of the simulations conducted to determine the generalized Sobol' indices when applying the scaled US06 drive cycle current profile. Most of the voltage responses seem to lie between 3.5 – 4.0 V, while some samples reach significantly lower voltages, a few even being deeply discharged to voltages of around 2 V for short time spans (Fig. 7b). In the case of a real cell, discharging below the lower cutoff voltage of around 2.5 V, depending on cell chemistry, may cause irreversible damage [58]. However, since the DFN model does not account for any of these degradation mechanisms, cell behavior is not altered by low cell voltages.

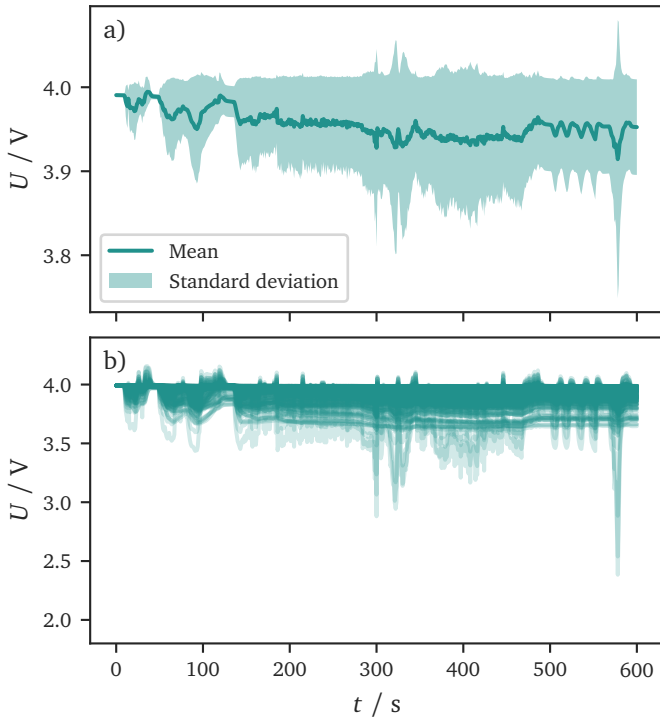


Figure 7: Output of the DFN model for the scaled US06 drive cycle for different parameter samples depicted as a) the mean and standard deviation over 10000 samples and b) individual voltage responses for 500 samples.

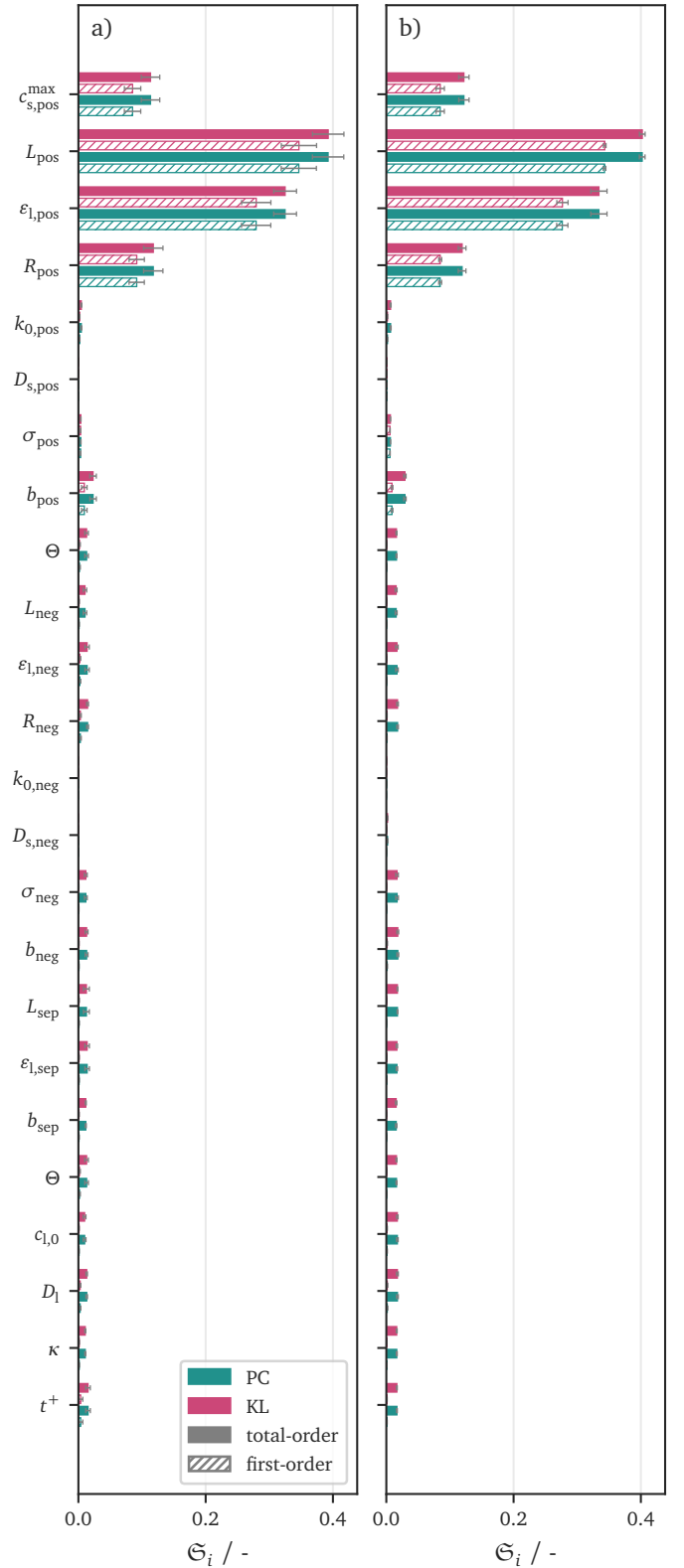


Figure 8: Generalized Sobol' indices obtained via three runs of sensitivity analysis with two different PC expansion truncation strategies, namely a) a full PC expansion of order 2 with 10000 samples, $N_{KL} = 10$, and OLS regression; and b) a sparse PC expansion of order 5 with $q = 0.7$, 70000 samples, $N_{KL} = 10$, and OLS regression. The error bars signify the standard deviation of three individual runs.

Based on the variance caused in the voltage response by the randomly sampled parameter vectors, we can obtain generalized Sobol' indices that aggregate the effects of each parameter on the model output over the whole time interval. The results of the complete sensitivity analysis over all considered parameters with a full and a sparse PC expansion are shown in Fig. 8. We show the results obtained via OLS regression, because we did not find any significant differences between LARS and OLS (Fig. B.12). Unexpectedly, even for smaller sample sizes, LARS did not perform significantly better than OLS. We find that the capacity-determining parameters of the cathode, i.e., $c_{s,\text{pos}}^{\text{max}}$, L_{pos} , $\varepsilon_{1,\text{pos}}$, together with the positive electrode particle radius R_{pos} are responsible for almost all the variance in the voltage response, overshadowing the sensitivity of the remaining parameters. L_{pos} is hereby the most influential parameter, closely followed by $\varepsilon_{1,\text{pos}}$, while R_{pos} and $c_{s,\text{pos}}^{\text{max}}$ each only amount to less than half the sensitivity of the more sensitive parameters. The difference in first-order and total-order indices is generally smaller than 0.1, indicating a limited role of constructive — i.e., purely variance increasing and non-compensating — parameter interactions on the voltage variance. While it does seem as if some of the obfuscated insensitive parameters have total-order indices close to zero, suggesting that these are even more insignificant than those with slightly visible total-order indices, the size and uniformity of the small total-order indices as well as the practical nonexistence of corresponding first-order indices challenges that assumption. It is therefore necessary to consult the subgroup analysis (Section 4.2) to further resolve the influence of the lowly sensitive parameters.

The predominant generalized Sobol' indices of these positive electrode parameters lie within expectation for multiple reasons: Firstly, the capacity-related parameters of the limiting electrode directly influence the full cell capacity and thereby the rate of change of the voltage when applying a current. Since the positive electrode is the limiting electrode in over 60% of samples (Fig. 6), this means that the positive electrode has a higher influence on the overall cell capacity and therefore a higher influence on the cell voltage. This capacity-induced change in the voltage of the cell tends to be much higher than those from overpotentials due to transport limitations or similar effects. Moreover, the OCV of the positive electrode extends over a larger voltage window and has a tendentially steeper slope. Since the overall cell voltage is the difference between the potential of the positive and negative electrode, the voltage will change more drastically when the positive electrode is the limiting electrode. Finally, the influence of R_{pos} , which is wholly unrelated to the capacity of the cell, most probably stems from its relation to the specific surface area of the electrode. In the DFN model, the specific surface area a_{pos} is computed via

$$a_{\text{pos}} = 3 \frac{\varepsilon_{s,\text{pos}}}{R_{\text{pos}}} \quad (47)$$

and governs the current density at the electrode-electrolyte interface. Increasing the current density leads to higher over-

potentials in the electrode, influencing the cell voltage. Seemingly, this effect is much more pronounced in the positive electrode, hinting at a tendency of lower overpotentials in the negative electrode. The particle radius additionally determines the diffusion path length of the intercalated lithium, which presents another mode of influence on the overpotential.

While the above does not constitute substantially novel insight into the DFN model, the results are interesting methodologically. First and foremost, they show that battery dynamics apparently produce low-rank processes, which lend themselves to sensitivity analysis via spectral representations. This is deducible from the close agreement of the generalized Sobol' indices obtained from both methods in Fig. 8 as well as the spectral decay of the eigenvalues, which is not shown here. This is an enormous advantage, because the KL method is much more efficient than the PC method. For our problem, where each of the 601 time steps is needed as a quadrature node due to insufficient smoothness of the output, the KL method needs to compute and store only about 1.7% of the number of coefficients used in the PC method. This is because the required number of surrogate models is reduced from 601 to 10. Depending on the number of cores available, this reduction can lead to solving the regression problem for all PC surrogate models in parallel, thereby significantly speeding up the procedure. This enables the use of higher order PC expansions for the KL method, since the number of coefficients is the limiting factor memory-wise. We observe that full lower order expansions yield comparable results to sparse higher order expansions for the generalized Sobol' indices. Higher-order PC expansions typically lead to more expressive surrogate models and lower surrogate model errors. Minimizing the surrogate model error is seemingly not immediately relevant for the analysis, but a low error might prove valuable for subsequent use cases of the surrogate model (Section 5). By comparison of the full (Fig. 8a) and the sparse PC expansion (Fig. 8b), we can also see that the choice of the hyperbolic cross truncation coefficient did not overly eliminate any relevant interaction terms in the expansion, since the total-order indices closely agree between the full and the sparse expansion, further substantiating that the sparsity-of-effects principle holds true.

We obtain estimates of the optimal number of samples (Appendix B) for the full second order PC expansion of $N = 7475$ and $N = 68379$ for the sparse PC expansion of order 5 with a cross truncation coefficient of $q = 0.7$. This reveals that both analyses are provided with a sufficient number of samples. The error bars, however, do differ significantly between the analysis conducted with a sparse PC expansion and the analysis done with a full PC expansion. This likely stems from the much higher sample volume per run in the sparse case.

4.2. Subgroup analysis

Fig. 9 shows the mean generalized Sobol' indices resulting from the subgroup sensitivity analysis where out-of-group parameters were varied over a space-filling design of LHS points. The error bars signify the variability of the indices

when conducting the analysis at different points in parameter space. Since the scales are no longer coupled by a common total variance, we can not directly compare the magnitude of the indices between groups. For that reason, we have to take into consideration the mean caused variance per group \bar{D} , which offers a semi-quantitative hierarchical ordering of the groups (Fig. 10). We can see that the results of the subgroup analysis, together with the maximum caused variance, align well with the full analysis. The group of capacity-related positive electrode parameters causes the largest variance in the voltage response, akin to the full analysis, where most of the total variance is attributed to those same parameters. Similarly, the only parameter not related to the capacity with significant influence in the full analysis R_{pos} is found to be the most important member in the group with the second highest variance. These observations suggest that the subgroup analysis does not yield contrasting results to the full analysis. Since the differences between first- and total-order indices in the subgroups tend to overall be rather small, and we assume inter-group interactivity to be much less relevant than intra-group interactivity due to our domain-based grouping, we believe that the interactive terms lost by subgrouping are negligible. Using the information provided by Fig. 8, Fig. 9, and Fig. 10 lets us better resolve the coarse relative importance ranking provided by the full analysis.

Some of the indices in Fig. 9 come with high standard deviations, sometimes even higher than their mean value, e.g., in the case of $c_{1,0}$ and σ_{neg} . This variability stems from the variation in the fixed out-of-group parameters and indicates changes in the physical behavior of the DFN model depending on the location in parameter space. An example of this could be b_{neg} , which controls the tortuosity of the negative electrode and is therefore highly important when lithium ion transport through the liquid phase in the porous negative electrode is the main limitation, but less relevant when other effects are limiting. In a full analysis, all of those cases are taken into account automatically, but in the subgroup analysis this is only emulated by averaging over different locations in parameter space. Nevertheless, the subgroup analysis is a very efficient way of complementing the full analysis to obtain more highly resolved hierarchical information.

Special consideration has to be given to the interpretation of the sensitivity indices of the capacity-related parameters. Akin to the full analysis, the positive electrode is capacity-limiting in most cases. Specifically, out of all the 30 analyses of group 1, approximately two thirds were dominated by a majority, i.e., over 50%, of samples with a capacitively smaller positive electrode. The spread to lower variance values of group 1 in Fig. 10 can likely be attributed to the other third, in which the positive electrode parameters are less influential by virtue of not being capacitively limiting. Group 3, i.e., the group of capacity-related parameters of the negative electrode, has significantly lower caused variance values compared to group 1. This is explainable by the lower number of analyses of group 3 with a majority of samples with a capacitively smaller negative electrode as well as the lower OCV range in the negative electrode, causing a smaller voltage change even when

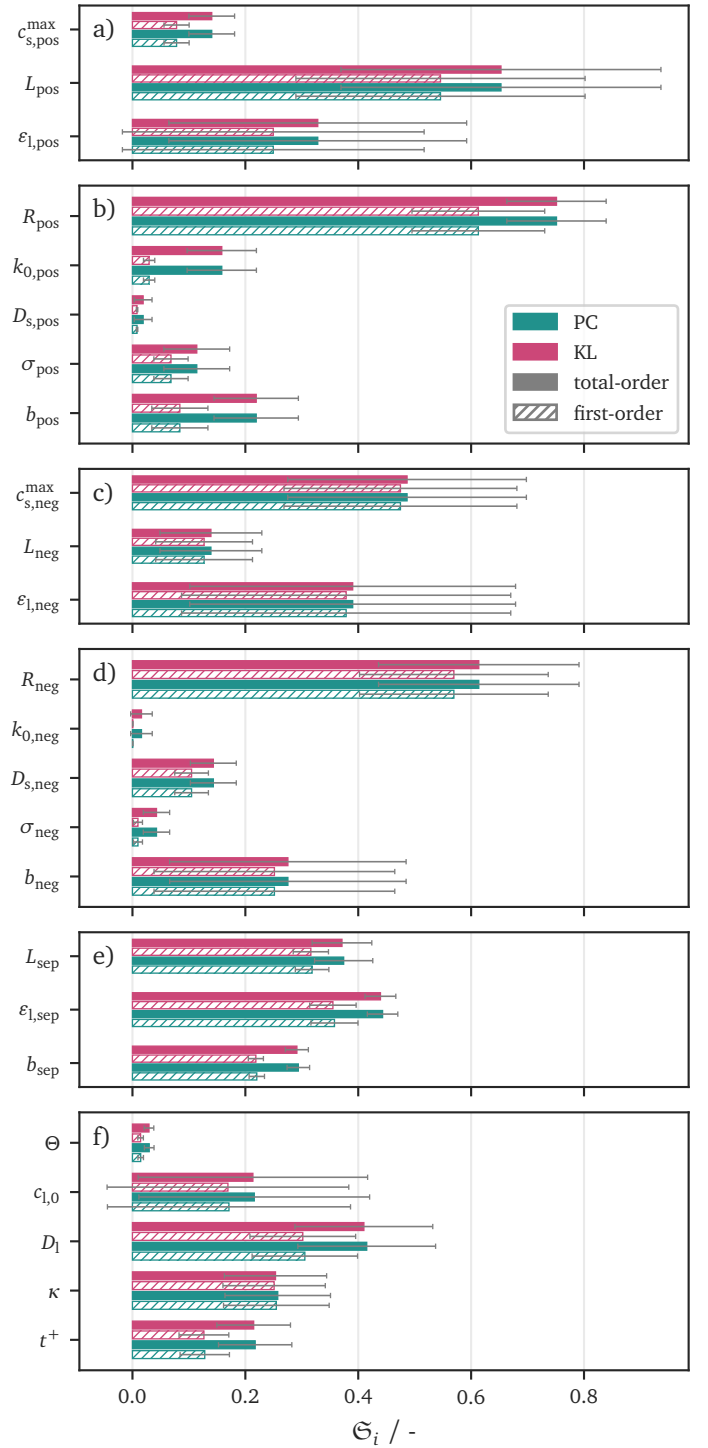


Figure 9: Results of the subgroup analysis for the six considered parameter groups, namely a) the capacity-related parameters of the positive electrode, b) the non-capacity-related parameters thereof, c) the capacity-related parameters of the negative electrode, d) the non-capacity-related parameters thereof, e) the separator-related parameters, and f) the electrolyte-related parameters. Each sensitivity analysis was conducted using a full PC expansion of order 6 with 10000 samples, $N_{\text{KL}} = 10$, and OLS regression. The error bars indicate the spread of the generalized Sobol' indices over the 30 different out-of-group parameter variations, which span over a design of space-filling LHS points.

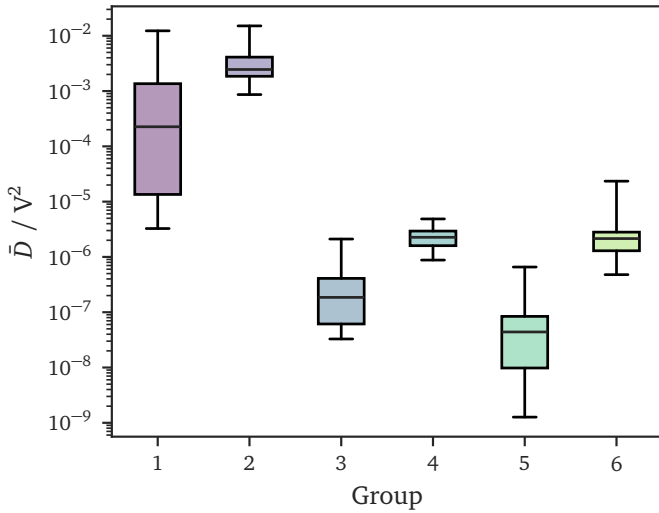


Figure 10: Boxplots of the mean caused variance in the voltage response per group over the 30 conducted sensitivity analyses with 10000 parameter samples. The mean caused variance \bar{D} is the average of the variance over the whole time window of the model response. The group numbers refer to the groups in Tab. 1, where 1 stands for the capacity-related parameters of the positive electrode, 2 stands for the non-capacity-related parameters of the positive electrode, 3 and 4 are the capacity-related and non-capacity-related parameters of the negative electrode respectively, 5 includes the separator-related parameters, and 6 contains the electrolyte-related parameters.

the negative electrode is capacitively limiting. Additionally, the relative importances in group 3 are presumably slightly skewed by the potentially insufficient range of L_{neg} obtained from the LiionDB (Fig. 5). These aspects, together with the fact that, while less relevant for the voltage variance, the capacity of the non-limiting electrode is still highly relevant for the OCV balancing of the model and should not be unduly neglected, make the interpretation of variance-based sensitivity analysis complicated for capacity-related parameters. A potential workaround could be scaling the current profile for each parameter sample individually, thereby eliminating the influence of the capacity on the voltage response. This would also rid the dominance of capacity effects from the full analysis, potentially eliminating the need for a subgroup analysis. Future research could be directed at the feasibility and implications of a sensitivity analysis with individually scaled load profiles.

Furthermore, some general trends appear to emerge from the results. It seems as if in the negative electrode, charge transfer limitation rarely occurs, since the reaction rate constant, which drives the exchange current density, has barely any impact in its group. Conversely, in the positive electrode, the reaction rate constant does play a role, but the effect of the solid diffusivity seems negligible, indicating a subordinate role of solid diffusion limitation. This would likely be different for load profiles with longer consecutive charging or discharging times or with larger current densities because charge transfer or solid diffusion limitations would have an

overall bigger impact on the dynamics of the cell.

4.3. Parameter fixing and error estimation

Alexanderian et al. [30] discuss the role of the generalized Sobol' indices as a priori error bounds for the loss of total variance when fixing unimportant parameters to some nominal values inside the corresponding bounds. From the viewpoint of battery model parametrization, we are less interested in the loss of variance of the stochastic model and would rather know about the error introduced to a parametrized battery model with deterministic parameter values when setting the unimportant parameters to some random value inside their bounds. This is to emulate the common practice in battery modelling of setting some parameters to arbitrary values from literature, and investigate its influence on the model error. To this end, we employ the base parametrization to simulate the unscaled version of the US06 drive cycle and vary increasingly more insensitive parameters to examine the resulting model error. The model error in this case is the deviation from the reference result obtained with the base parametrization. The seven most insensitive parameters determined above consist of b_{sep} , L_{sep} , $\epsilon_{1,\text{sep}}$, $k_{0,\text{neg}}$, σ_{neg} , Θ , and t^+ . In the following, the insensitive parameters are always varied over 100 samples.

Fig. 11 shows the results of selecting random values for an increasing number of insensitive parameters and comparing the voltage response to the reference output. When varying the three least sensitive parameters, i.e., b_{sep} , L_{sep} , and $\epsilon_{1,\text{sep}}$, the mean absolute error (MAE) mostly stays below 25 mV (Fig. 11d) and the average root mean squared error (RMSE) over all simulations is 11.2 mV. For random variations of the five least sensitive parameters, the MAE largely stays around 25 mV (Fig. 11e) and the average RMSE amounts to 17.0 mV. Setting the seven least important parameters to random values inside their respective intervals causes an MAE above 100 mV (Fig. 11f) and an average RMSE of 53.6 mV.

These results underscore the low impact of changes in insensitive parameters on the model response and show that the methodology outlined above yields valid sensitivity information over the whole time interval. However, it also exemplifies a shortcoming: sensitivity information is always related to a simulative scenario, a certain load profile, etc., and is also influenced by our choice of the distribution for the parameter values. This hinders general statements on relative parametric importance, because one might be able to devise a load profile which leads to wholly different parametric sensitivities by design. However, since models are usually employed for certain use cases and only parametrized and validated for these use cases, one should generally be able to investigate the parametric sensitivity for select representative scenarios of battery model use (e.g., fast charging, discharging, and a drive cycle for use in the automotive sector) to get a good understanding of which parameters are less influential in the region of model validity. Instead of using very general uniform parameter bounds, one might also choose normally distributed parameters taking into account some experimental error. This can answer the question which parameter's error contributes most to the battery model's uncertainty, in order to potentially

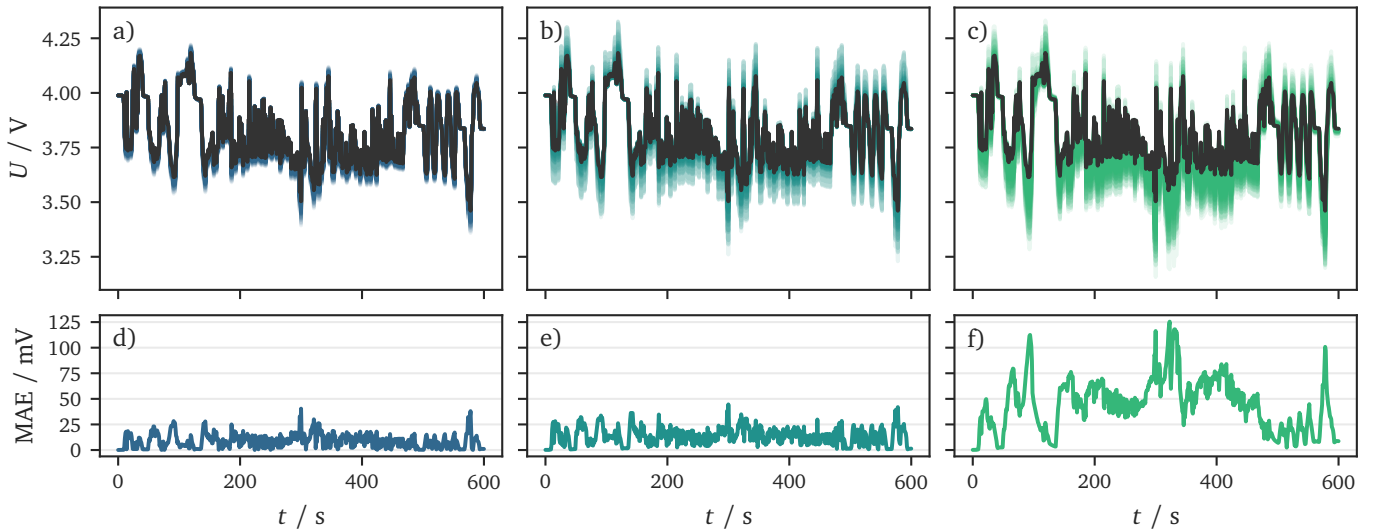


Figure 11: Comparison of the voltage responses obtained via the base parametrization and when varying an increasing amount of insensitive parameters. The voltage curve comparison for a) three ($b_{\text{sep}}, L_{\text{sep}}, \epsilon_{1,\text{sep}}$), b) five ($b_{\text{sep}}, L_{\text{sep}}, \epsilon_{1,\text{sep}}, \sigma_{\text{neg}}, k_{0,\text{neg}}$), and c) seven ($b_{\text{sep}}, L_{\text{sep}}, \epsilon_{1,\text{sep}}, \sigma_{\text{neg}}, k_{0,\text{neg}}, \Theta, t^+$) insensitive parameters as well as the corresponding mean absolute error plots for variations in the d) three, e) five, and f) seven least influential parameters substantiate the results of the subgroup analysis.

remeasure said parameter to decrease the error and improve the model. The generalized investigation of the input-output relations of the DFN model is of course also limited by the differences in cell chemistry. While a cell with an NMC positive electrode and a graphite negative electrode exhibits an OCV with a significant slope for every state of charge, a LiFePO₄ positive electrode typically plateaus in medium ranges of the state of charge. This affects the model behavior in numerous ways and is difficult to consider concomitantly in a sensitivity study.

Finally, we would generally advise against considering capacity-related parameters as insensitive from the above study. As aforementioned, the interplay of the capacity related parameters with the electrode and total cell capacity is complicated and not immediately visible in a large voltage variance. Nevertheless, the quality of the model highly depends on correct capacitive balancing, which stems from the combination of the capacity-related parameters of both electrodes. To alleviate this problem in potential future studies with broad parameter ranges, one could be conducting sensitivity studies with individually scaled load profiles, to nullify the effect of capacity change on the voltage response and thereby yield capacity-agnostic sensitivities.

5. Conclusion and outlook

Efficient and accurate sensitivity analysis of nonlinear electrochemical battery models is of high relevance for a variety of use cases and research questions. This work restated the problem regarding the inadequacy of OAT methods, discussed the present restriction of readily available global sensitivity analysis methods to scalar quantities of interest, and implemented

novel approaches by Alexanderian et al. [30] for global sensitivity analysis of time-dependent model outputs. We applied the methods to the simulation of a drive cycle with the DFN model and determined generalized Sobol' indices by a full analysis and a subgroup analysis to further resolve the influence of lowly sensitive parameters. We found that battery models seemingly produce low rank processes, which lend themselves to efficient time-dependent global sensitivity analysis via spectral representations. Specifically, the KL method produced comparable results to the PC method at approximately one hundredth of the memory requirements. The computational cost can be lowered even further by the use of sparse PC expansions. In cases where the low rank process requirement might not be met, the PC method would be the preferred choice. Moreover, subsequent simulations with random values inserted for an increasing number of unimportant parameters revealed a direct correlation to the model error, corroborating the sensitivity analysis results and suggesting potential applications in battery model parametrization.

Unfortunately, sensitivity indices are dependent on the chosen load profile and the selected parameter distributions, which limits the generalizability of the results and makes it hard to derive universal input-output relations of the DFN model. However, we were able to determine certain pitfalls in variance-based sensitivity analysis of electrochemical battery models, with the hope of providing some guidance in employing this method as a helpful tool in the field of simulative battery research.

Overall, this work presents an important step towards efficient and accurate sensitivity analyses for time-dependent quantities in simulation-based battery research and beyond. The presented methodology enables researchers to determine

model parameters of special interest for factor prioritization via generalized first-order Sobol' indices, and less influential parameters for factor fixing via generalized total-order Sobol' indices. Research questions concerned with the main factors driving some model behavior over time can therefore be addressed more easily and adequately. This is especially relevant for model-based design studies, where the parameters of physical systems are optimized using well-validated simulation models, because the most influential parameters can be identified more reliably. One such example would be model-based cell design using the DFN model.

Further research could be directed towards the feasibility of capacity-agnostic sensitivity analyses of electrochemical battery models with individually scaled load profiles. More sophisticated models, e.g., the DFN model coupled to a thermal model to account for heat generation and temperature dependence, should be investigated in future sensitivity studies to be able to more realistically describe cell behaviour. Extending the approach to be able to account for functional dependencies of parameters would be a worthwhile feature in this context. Additionally, the created surrogate models with a low enough approximation error might be employed in downstream tasks where cheap function evaluations are required, e.g., optimization, potentially with a multifidelity ansatz. Moreover, one could investigate alternative implementational choices, e.g., a different quadrature rule for the treatment of the time integrals in the computation of the generalized Sobol' indices, different optimization algorithms for the determination of the PC coefficients or employing the pseudo-spectral approach for computing PC coefficients.

Declaration of competing interest

Michele Spinola and Christoph Weißinger are employees at Capgemini Engineering. The remaining authors declare that the research was conducted in the absence of any commercial or financial relationships that could be construed as a potential conflict of interest.

CRedit authorship contribution statement

Elia Zonta: Conceptualization, Methodology (lead), Software, Formal analysis (equal), Investigation, Data curation, Writing - original draft, Visualization. **Ivana Jovanovic Buha:** Methodology (supporting), Formal analysis (equal), Writing - review & editing. **Michele Spinola:** Writing - review & editing, Project administration. **Christoph Weißinger:** Writing - review & editing, Supervision, Funding acquisition. **Hans-Joachim Bungartz:** Writing - review & editing, Supervision. **Andreas Jossen:** Writing - review & editing, Supervision, Funding acquisition.

Acknowledgements

This work is supported by Capgemini in the context of the TUM-Capgemini Research and Development Agreement "Innovative and non-invasive methods of parameter identification

for lithium-ion battery models". The authors would like to thank Johannes Natterer, Alexander Frank, and Axel Durdel for fruitful discussions.

Appendix A. Considered parameter ranges

Tab. A.2 summarizes the parameter distributions that were used to conduct sensitivity analysis throughout this work.

Appendix B. Influence of sample size and choice of regression algorithm

Fig. B.12 shows the results of a small robustness study concerning the time-dependent global sensitivity analysis. We investigated the influence of the number of samples and of the two different regression algorithms on the outcome of the sensitivity analysis over three individual runs each.

Sudret [36] provides an empirical estimate for the optimal number of samples for PC-based surrogate models, given as

$$N = (d - 1)N_{\text{PC}}, \quad (\text{B.1})$$

where the number of PC terms or coefficients can be computed for full expansions as

$$N_{\text{PC}} = \frac{(d + p)!}{d!p!}. \quad (\text{B.2})$$

This lets us compute the optimal number of samples for the robustness study as $N = 7475$. We can see that above this sample size threshold, the results vary only slightly, while the analysis with a sample size of $N = 1000$ appears to be significantly undersampled.

The results obtained with OLS and LARS regression appear to be almost equivalent, irrespective of sample size.

Appendix C. Comparison of one-at-a-time sensitivity analysis and generalized Sobol' indices

To better illustrate the theoretical considerations made in section 2.1.1, we compare the result of one-at-a-time sensitivity analysis with the generalized Sobol' indices used throughout this work for a damped oscillator example from literature [30], whose displacement y is governed by an initial value problem of the form

$$\begin{aligned} y'' + 2\alpha y' + (\alpha^2 + \beta^2)y &= 0, \\ y(0) &= \ell, \quad y'(0) = 0, \end{aligned} \quad (\text{C.1})$$

where $\alpha \sim \mathcal{U}(\frac{3}{8}, \frac{5}{8})$, $\beta \sim \mathcal{U}(\frac{10}{4}, \frac{15}{4})$, $\ell \sim \mathcal{U}(-\frac{5}{4}, -\frac{3}{4})$ are considered uncertain parameters with uniform distributions. For this comparison, we employ the OAT sensitivity metric from Li et al. [11], namely

$$S_{i,\text{OAT}} = \sqrt{\frac{1}{N_s} \sum_{j=1}^{N_s} (y_{ij} - \bar{y}_i)^2}, \quad (\text{C.2})$$

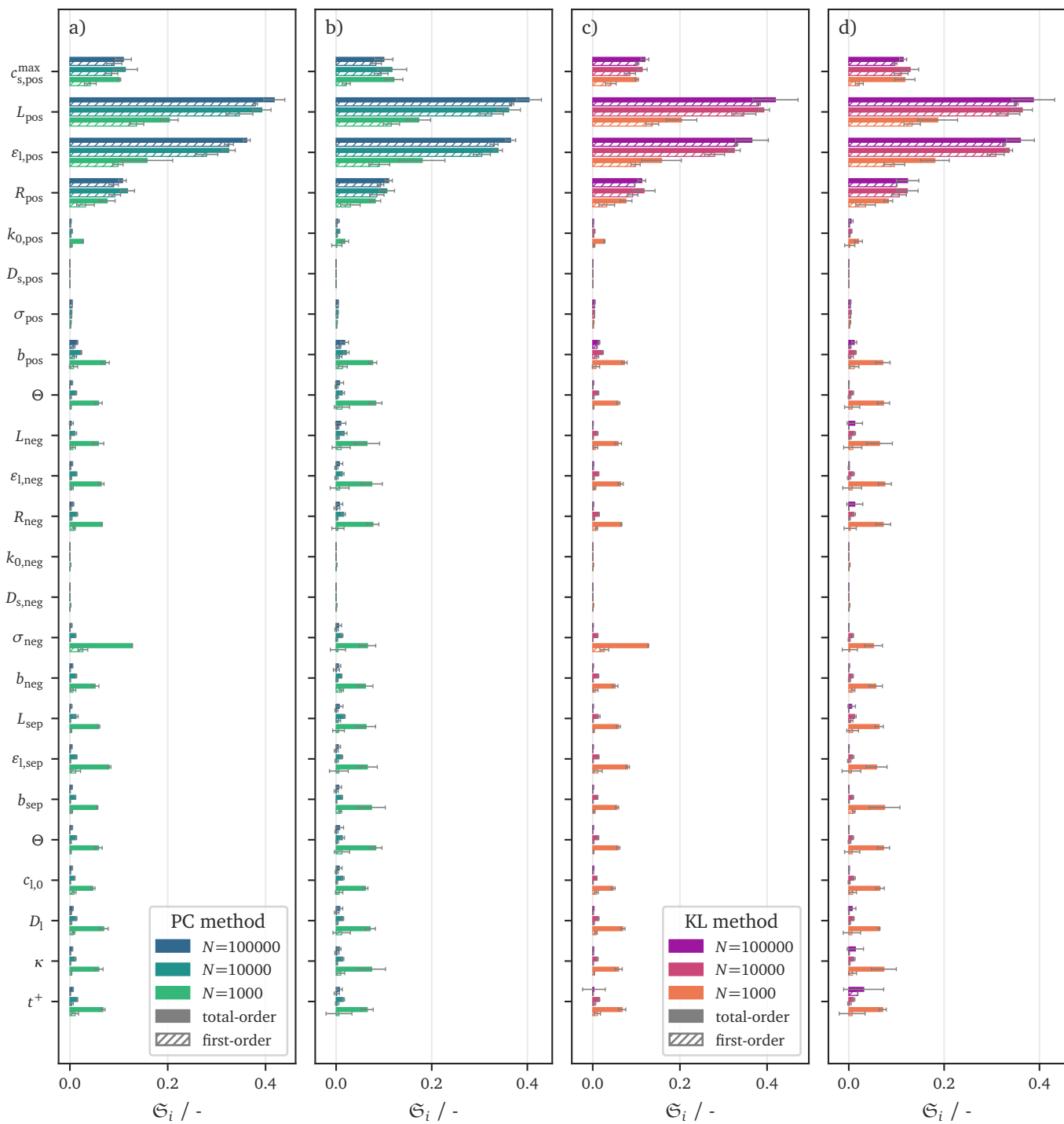


Figure B.12: Results of different sensitivity analyses with a full PC expansion of order 2, varying sample sizes, $N_{\text{KL}} = 10$, using a) the PC method with OLS regression, b) the PC method with LARS regression, c) the KL method with OLS regression, and d) the KL method with LARS regression.

Table A.2: Numerical values of the parameter ranges used throughout this work.

Name	Symbol	Unit	Min.	Max.	Distribution
Positive electrode max, concentration	$c_{s, \text{pos}}^{\text{max}}$	mol m^{-3}	23900	51765	Uniform
Positive electrode thickness	L_{pos}	m	$6.00 \cdot 10^{-6}$	$6.60 \cdot 10^{-5}$	Uniform
Positive electrode porosity	$\epsilon_{l, \text{pos}}$	-	0.171	0.648	Uniform
Positive electrode particle radius	R_{pos}	m	$5.00 \cdot 10^{-7}$	$1.00 \cdot 10^{-5}$	Uniform
Positive electrode reaction rate constant	$k_{0, \text{pos}}$	$\text{m}^{2.5} \text{mol}^{-0.5} \text{s}^{-1}$	$2.10 \cdot 10^{-12}$	$2.41 \cdot 10^{-5}$	Loguniform
Positive electrode diffusivity	$D_{s, \text{pos}}$	$\text{m}^2 \text{s}^{-1}$	$9.59 \cdot 10^{-19}$	$2.51 \cdot 10^{-12}$	Loguniform
Positive electrode conductivity	σ_{pos}	S m^{-1}	$5.20 \cdot 10^{-6}$	$1.00 \cdot 10^3$	Loguniform
Positive electrode Bruggeman coefficient	b_{pos}	-	1.44	2.44	Uniform
Negative electrode max, concentration	$c_{s, \text{neg}}^{\text{max}}$	mol m^{-3}	16100	31920	Uniform
Negative electrode thickness	L_{neg}	m	$4.60 \cdot 10^{-5}$	$7.20 \cdot 10^{-5}$	Uniform
Negative electrode porosity	$\epsilon_{l, \text{neg}}$	-	0.26	0.50	Uniform
Negative electrode particle radius	R_{neg}	m	$1.00 \cdot 10^{-5}$	$1.26 \cdot 10^{-5}$	Uniform
Negative electrode reaction rate constant	$k_{0, \text{neg}}$	$\text{m}^{2.5} \text{mol}^{-0.5} \text{s}^{-1}$	$1.00 \cdot 10^{-11}$	$3.00 \cdot 10^{-3}$	Loguniform
Negative electrode diffusivity	$D_{s, \text{neg}}$	$\text{m}^2 \text{s}^{-1}$	$2.00 \cdot 10^{-16}$	$9.07 \cdot 10^{-12}$	Loguniform
Negative electrode conductivity	σ_{neg}	S m^{-1}	$1.11 \cdot 10^{-1}$	$2.20 \cdot 10^3$	Loguniform
Negative electrode Bruggeman coefficient	b_{neg}	-	1.50	4.10	Uniform
Separator thickness	L_{sep}	m	$1.60 \cdot 10^{-5}$	$5.00 \cdot 10^{-5}$	Uniform
Separator porosity	$\epsilon_{l, \text{sep}}$	-	0.37	0.60	Uniform
Separator Bruggeman coefficient	b_{sep}	-	1.50	2.57	Uniform
Thermodynamic factor	Θ	-	1.00	1.86	Uniform
Initial electrolyte concentration	$c_{l, 0}$	mol m^{-3}	500	1500	Uniform
Electrolyte diffusivity	D_l	$\text{m}^2 \text{s}^{-1}$	$3.60 \cdot 10^{-11}$	$1.09 \cdot 10^{-9}$	Loguniform
Electrolyte ionic conductivity	κ	S m^{-1}	$4.45 \cdot 10^{-3}$	2.45	Uniform
Transference number	t^+	-	-0.37	0.51	Uniform

where y_{ij} is the displacement when changing a parameter i to a certain level j , \bar{y}_i is the average over the displacements for all levels of a certain parameter, and N_s is the number of levels. We set $N_s = 2$ and use the bounds of the uniform distribution for each parameter. Since y is a function of time, we obtain one $S_{i, \text{OAT}}$ per parameter for each point in time. Generalized Sobol' indices are obtained using the PC method using 100 quadrature nodes in time, PC expansions of order 4, and 100 random samples. Fig. C.13 compares the results of both methods.

The displacement obtained when varying each parameter individually to its minimum and maximum values shows that the attainable maximum and minimum displacements are underestimated (Fig. C.13a). When parameters are varied in tandem, the displacement reaches lower minima and higher maxima, especially in the early phase (Fig. C.13b). This means that the possible amplitude of the model response in the given parameter space is underestimated when parameters are only varied individually. Comparing the different sensitivity indices reveals that they show similar trends, which stems from the rather weak coupling of the parameters in the damped oscillator example. However, the pointwise-in-time $S_{i, \text{OAT}}$ values lack conclusive interpretability, because the ranking of parametric importance differs at each point in time. Contrastingly, generalized Sobol' indices at a certain time point t aggregate the parametric effects of the whole interval $[0, t]$,

making their interpretation straightforward and yielding a single metric describing the normalized sensitivity over the whole time interval.

For battery models, which generally exhibit much stronger nonlinear coupling between the parameters, the differences in model output observed in Fig. C.13a and b will be exacerbated. The agreement in trend between OAT and generalized Sobol' indices will generally also decrease with increasing nonlinear coupling between model parameters.

Fig. C.13d has the additional merit of showing that our implementation of the method correctly reproduces the original results of Alexanderian et al. [30, Fig. 2].

References

- [1] S. Chu, A. Majumdar, Opportunities and challenges for a sustainable energy future, *Nature* 488 (7411) (2012) 294–303. doi:10.1038/nature11475.
- [2] F. Oehler, X. Deuschl, K. Nürnberger, A. Graule, S. Kücher, T. Roth, A. Adam, J. Li, R. Mörtel, A. Jossen, Online adaptive anode potential-controlled fast charging of lithium-ion cells using a validated electrochemical model-based virtual reference electrode, *Journal of Power Sources* 608 (2024) 234620. doi:10.1016/j.jpowsour.2024.234620.

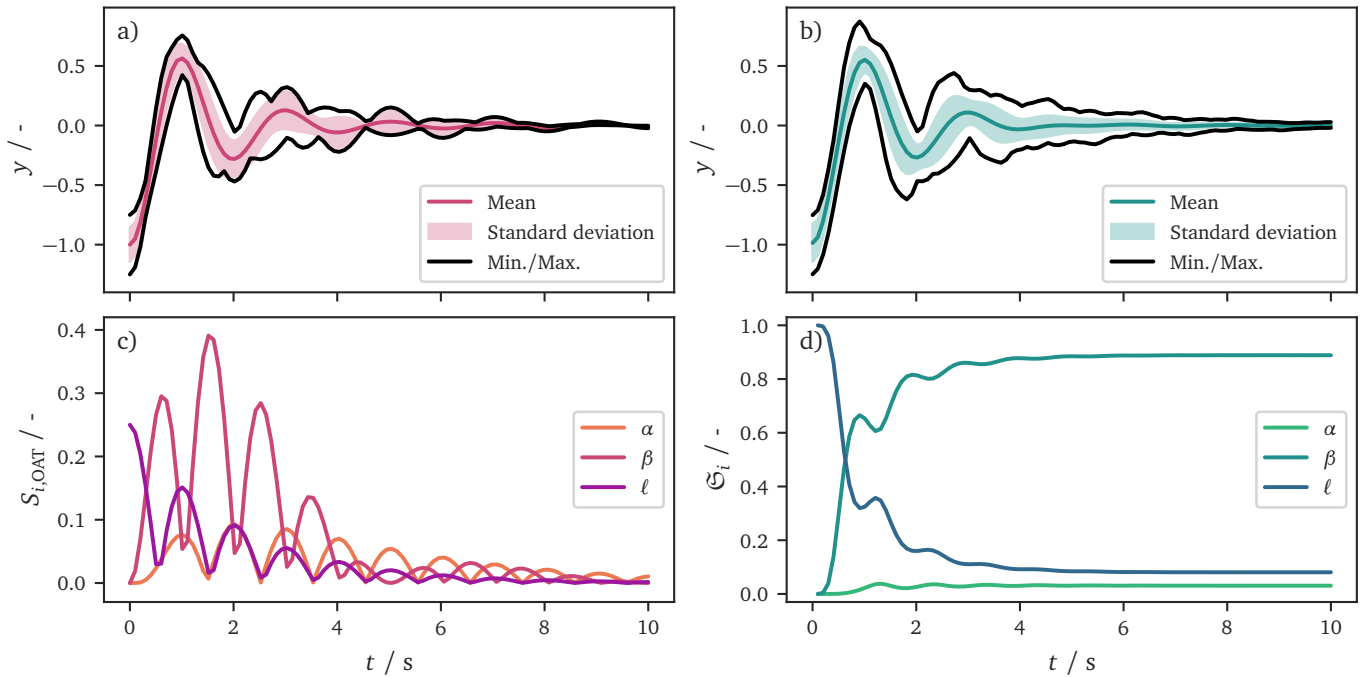


Figure C.13: Comparison of OAT sensitivity with generalized Sobol' indices. The upper row shows the damped harmonic oscillator displacement obtained from a) varying each parameter individually to its minimum and maximum value and b) sampling 100 random parameter combinations. The lower row displays the corresponding c) OAT sensitivity metrics and d) generalized Sobol' indices.

- [3] M. Astaneh, J. Andric, L. Löfdahl, P. Stopp, Multiphysics simulation optimization framework for lithium-ion battery pack design for electric vehicle applications, *Energy* 239 (2022) 122092. doi:10.1016/j.energy.2021.122092.
- [4] X. Zhang, Y. Gao, B. Guo, C. Zhu, X. Zhou, L. Wang, J. Cao, A novel quantitative electrochemical aging model considering side reactions for lithium-ion batteries, *Electrochimica Acta* 343 (2020) 136070. doi:10.1016/j.electacta.2020.136070.
- [5] M. Doyle, T. F. Fuller, J. Newman, Modeling of Galvanostatic Charge and Discharge of the Lithium/Polymer/Insertion Cell, *Journal of The Electrochemical Society* 140 (6) (1993) 1526–1533. doi:10.1149/1.2221597.
- [6] T. F. Fuller, M. Doyle, J. Newman, Simulation and Optimization of the Dual Lithium Ion Insertion Cell, *Journal of The Electrochemical Society* 141 (1) (1994) 1–10. doi:10.1149/1.2054684.
- [7] A. Saltelli, K. Aleksankina, W. Becker, P. Fennell, F. Ferretti, N. Holst, S. Li, Q. Wu, Why so many published sensitivity analyses are false: A systematic review of sensitivity analysis practices, *Environmental Modelling & Software* 114 (2019) 29–39. doi:10.1016/j.envsoft.2019.01.012.
- [8] A. Saltelli, P. Annoni, How to avoid a perfunctory sensitivity analysis, *Environmental Modelling & Software* 25 (12) (2010) 1508–1517. doi:10.1016/j.envsoft.2010.04.012.
- [9] C. Edouard, M. Petit, C. Forgez, J. Bernard, R. Revel, Parameter sensitivity analysis of a simplified electrochemical and thermal model for Li-ion batteries aging, *Journal of Power Sources* 325 (2016) 482–494. doi:10.1016/j.jpowsour.2016.06.030.
- [10] Y. Bi, S.-Y. Choe, Automatic Estimation of Parameters of a Reduced Order Electrochemical Model for Lithium-Ion Batteries at the Beginning-of-Life, in: 2018 IEEE Vehicle Power and Propulsion Conference (VPPC), IEEE, Chicago, IL, 2018, pp. 1–6. doi:10.1109/VPPC.2018.8604954.
- [11] W. Li, D. Cao, D. Jöst, F. Ringbeck, M. Kuipers, F. Frie, D. U. Sauer, Parameter sensitivity analysis of electrochemical model-based battery management systems for lithium-ion batteries, *Applied Energy* 269 (2020) 115104. doi:10.1016/j.apenergy.2020.115104.
- [12] Y. Liu, S. Tang, L. Li, F. Liu, L. Jiang, M. Jia, Y. Ai, C. Yao, H. Gu, Simulation and parameter identification based on electrochemical-thermal coupling model of power lithium ion-battery, *Journal of Alloys and*

- Compounds 844 (2020) 156003. doi:10.1016/j.jallcom.2020.156003.
- [13] J. Vazquez-Arenas, L. E. Gimenez, M. Fowler, T. Han, S.-k. Chen, A rapid estimation and sensitivity analysis of parameters describing the behavior of commercial Li-ion batteries including thermal analysis, *Energy Conversion and Management* 87 (2014) 472–482. doi:10.1016/j.enconman.2014.06.076.
- [14] L. Zhang, C. Lyu, G. Hinds, L. Wang, W. Luo, J. Zheng, K. Ma, Parameter sensitivity analysis of cylindrical LiFePO₄ battery performance using multi-physics modeling, *Journal of The Electrochemical Society* 161 (5) (2014) A762–A776. doi:10.1149/2.048405jes.
- [15] Y. Wang, J. Li, S. Guo, M. Sun, H. Zhao, Y. Wu, L. Zhao, Z. Wang, Parameter sensitivity analysis of a multi-physics coupling aging model of lithium-ion batteries, *Electrochimica Acta* 477 (2024) 143811. doi:10.1016/j.electacta.2024.143811.
- [16] W. Li, I. Demir, D. Cao, D. Jöst, F. Ringbeck, M. Junker, D. U. Sauer, Data-driven systematic parameter identification of an electrochemical model for lithium-ion batteries with artificial intelligence, *Energy Storage Materials* 44 (2022) 557–570. doi:10.1016/j.ensm.2021.10.023.
- [17] T.-C. Pan, E.-J. Liu, H.-C. Ku, C.-W. Hong, Parameter identification and sensitivity analysis of lithium-ion battery via whale optimization algorithm, *Electrochimica Acta* 404 (2022) 139574. doi:10.1016/j.electacta.2021.139574.
- [18] B. Wimmarshana, I. Bin-Mat-Arishad, A. Fly, Parameter sensitivity analysis of a physico-chemical lithium-ion battery model with combined discharge voltage and electrochemical impedance data, *Journal of Power Sources* 527 (2022) 231125. doi:10.1016/j.jpowsour.2022.231125.
- [19] X. Lai, S. Wang, S. Ma, J. Xie, Y. Zheng, Parameter sensitivity analysis and simplification of equivalent circuit model for the state of charge of lithium-ion batteries, *Electrochimica Acta* 330 (2020) 135239. doi:10.1016/j.electacta.2019.135239.
- [20] C. Chang, L. Chen, X. Liu, J. Jiang, Y. Jiang, A. Tian, Y. Gao, T. Wu, Electrochemical aging model of lithium-ion battery with impedance output and its parameter sensitivity analysis and identification, *Journal of Energy Storage* 86 (2024) 111277. doi:10.1016/j.est.2024.111277.
- [21] C. Rabissi, G. Sordi, A. Innocenti, A. Casalegno, Fast and reliable calibration of thermal-physical model of lithium-ion battery: a sensitivity-based method, *Journal of Energy Storage* 59 (2023) 106435. doi:10.1016/j.est.2022.106435.
- [22] L. Xu, X. Lin, Y. Xie, X. Hu, Enabling high-fidelity electrochemical P2D modeling of lithium-ion batteries via fast and non-destructive parameter identification, *Energy Storage Materials* 45 (2022) 952–968. doi:10.1016/j.ensm.2021.12.044.
- [23] Y. Zhao, M. Wei, D. Dan, J. Dong, E. Wright, Enhancing battery electrochemical-thermal model accuracy through a hybrid parameter estimation framework, *Energy Storage Materials* 72 (2024) 103720. doi:10.1016/j.ensm.2024.103720.
- [24] M. Scheller, A. Durdal, A. Frank, J. Kriegler, A. Jossen, Impact of Polymer Interlayers on All-Solid-State Battery Performance Using a Physicochemical Modeling Approach, *Journal of The Electrochemical Society* 171 (2) (2024) 020509. doi:10.1149/1945-7111/ad1e3e.
- [25] M. Streb, M. Ohrelus, M. Klett, G. Lindbergh, Improving Li-ion battery parameter estimation by global optimal experiment design, *Journal of Energy Storage* 56 (2022) 105948. doi:10.1016/j.est.2022.105948.
- [26] N. Lin, X. Xie, R. Schenkendorf, U. Krewer, Efficient Global Sensitivity Analysis of 3D Multiphysics Model for Li-Ion Batteries, *Journal of The Electrochemical Society* 165 (7) (2018) A1169–A1183. doi:10.1149/2.1301805jes.
- [27] T. Rütger, W. Hileman, G. L. Plett, M. S. Trimboli, M. A. Danzer, Demystifying the Distribution of Relaxation Times: A Simulation-Based Investigation into the Limits and Possibilities of Interpretation for Lithium-Ion Batteries, *Journal of The Electrochemical Society* 171 (6) (2024) 060508. doi:10.1149/1945-7111/ad4fe5.
- [28] C.-J. Ko, C.-W. Lu, K.-C. Chen, C.-H. Chen, Using partial discharge data to identify highly sensitive electrochemical parameters of aged lithium-ion batteries, *Energy Storage Materials* 71 (2024) 103665. doi:10.1016/j.ensm.2024.103665.
- [29] J. Chen, S. P. Mattus, W. Cao, D. U. Sauer, W. Li, Global sensitivity analysis towards non-invasive parameterization of the electrochemical-thermal model for lithium-ion batteries, *Advances in Applied Energy* 18 (2025) 100221. doi:10.1016/j.adapen.2025.100221.
- [30] A. Alexanderian, P. A. Gremaud, R. C. Smith, Variance-based sensitivity analysis for time-dependent processes, *Reliability Engineering & System Safety* 196 (2020) 106722. doi:10.1016/j.res.2019.106722.
- [31] A. A. Wang, S. E. J. O’Kane, F. Brosa Planella, J. L. Houx, K. O’Regan, M. Zyskin, J. Edge, C. W. Monroe, S. J. Cooper, D. A. Howey, E. Kendrick, J. M. Foster, Review of parameterisation and a novel database (LiionDB) for continuum Li-ion battery models, *Progress in Energy* 4 (3) (2022) 032004. doi:10.1088/2516-1083/ac692c.

- [32] S. Razavi, H. V. Gupta, What do we mean by sensitivity analysis? The need for comprehensive characterization of “global” sensitivity in Earth and Environmental systems models, *Water Resources Research* 51 (5) (2015) 3070–3092. doi:10.1002/2014WR016527.
- [33] V. Czitrom, One-Factor-at-a-Time versus Designed Experiments, *The American Statistician* 53 (2) (1999) 126–131. doi:10.1080/00031305.1999.10474445.
- [34] W. Hoeffding, A Class of Statistics with Asymptotically Normal Distribution, *The Annals of Mathematical Statistics* 19 (3) (1948) 293–325. doi:10.1214/aoms/1177730196.
- [35] I. Sobol’, Global sensitivity indices for nonlinear mathematical models and their Monte Carlo estimates, *Mathematics and Computers in Simulation* 55 (1-3) (2001) 271–280. doi:10.1016/S0378-4754(00)00270-6.
- [36] B. Sudret, Global sensitivity analysis using polynomial chaos expansions, *Reliability Engineering & System Safety* 93 (7) (2008) 964–979. doi:10.1016/j.res.2007.04.002.
- [37] A. Saltelli, P. Annoni, I. Azzini, F. Campolongo, M. Ratto, S. Tarantola, Variance based sensitivity analysis of model output. Design and estimator for the total sensitivity index, *Computer Physics Communications* 181 (2) (2010) 259–270. doi:10.1016/j.cpc.2009.09.018.
- [38] M. Hadigol, K. Maute, A. Doostan, On uncertainty quantification of lithium-ion batteries: Application to an LiC₆/LiCoO₂ cell, *Journal of Power Sources* 300 (2015) 507–524. doi:10.1016/j.jpowsour.2015.09.060.
- [39] P. G. Constantine, A. Doostan, Time-dependent global sensitivity analysis with active subspaces for a lithium ion battery model, *Statistical Analysis and Data Mining: The ASA Data Science Journal* 10 (5) (2017) 243–262. doi:10.1002/sam.11347.
- [40] V. Sulzer, S. G. Marquis, R. Timms, M. Robinson, S. J. Chapman, Python Battery Mathematical Modelling (PyBaMM), *Journal of Open Research Software* 9 (1) (2021) 14. doi:10.5334/jors.309.
- [41] PyBaMM documentation — PyBaMM v24.9.0 Manual, <https://docs.pybamm.org/>, accessed 15 October 2024.
- [42] S. G. Marquis, V. Sulzer, R. Timms, C. P. Please, S. J. Chapman, An Asymptotic Derivation of a Single Particle Model with Electrolyte, *Journal of The Electrochemical Society* 166 (15) (2019). doi:10.1149/2.0341915jes.
- [43] J. A. E. Andersson, J. Gillis, G. Horn, J. B. Rawlings, M. Diehl, CasADi: a software framework for nonlinear optimization and optimal control, *Mathematical Programming Computation* 11 (1) (2018) 1–36. doi:10.1007/s12532-018-0139-4.
- [44] R. Sheikholeslami, S. Razavi, A. Haghnegahdar, What should we do when a model crashes? Recommendations for global sensitivity analysis of Earth and environmental systems models, *Geoscientific Model Development* 12 (10) (2019) 4275–4296. doi:10.5194/gmd-12-4275-2019.
- [45] Joblib documentation, <https://joblib.readthedocs.io/en/stable/>, accessed 24 January 2025.
- [46] G. Blatman, B. Sudret, Adaptive sparse polynomial chaos expansion based on least angle regression, *Journal of Computational Physics* 230 (6) (2011) 2345–2367. doi:10.1016/j.jcp.2010.12.021.
- [47] D. C. Montgomery, *Design and Analysis of Experiments*, Eighth Edition, John Wiley & Sons, Inc, Hoboken, NJ, 2013.
- [48] J. Feinberg, H. P. Langtangen, Chaospy: An open source tool for designing methods of uncertainty quantification, *Journal of Computational Science* 11 (2015) 46–57. doi:10.1016/j.jocs.2015.08.008.
- [49] B. Efron, T. Hastie, I. Johnstone, R. Tibshirani, Least angle regression, *The Annals of Statistics* 32 (2) (2004). doi:10.1214/009053604000000067.
- [50] F. Pedregosa, G. Varoquaux, A. Gramfort, V. Michel, B. Thirion, O. Grisel, M. Blondel, P. Prettenhofer, R. Weiss, V. Dubourg, J. Vanderplas, A. Passos, D. Cournapeau, M. Brucher, M. Perrot, Édouard Duchesnay, Scikit-learn: Machine Learning in Python, *Journal of Machine Learning Research* 12 (85) (2011) 2825–2830.
- [51] S. Park, D. Kato, Z. Gima, R. Klein, S. Moura, Optimal Experimental Design for Parameterization of an Electrochemical Lithium-Ion Battery Model, *Journal of The Electrochemical Society* 165 (7) (2018) A1309–A1323. doi:10.1149/2.0421807jes.
- [52] Y. Gao, X. Zhang, C. Zhu, B. Guo, Global Parameter Sensitivity Analysis of Electrochemical Model for Lithium-Ion Batteries Considering Aging, *IEEE/ASME Transactions on Mechatronics* 26 (3) (2021) 1283–1294. doi:10.1109/TMECH.2021.3067923.
- [53] M. Gouverneur, F. Schmidt, M. Schönhoff, Negative effective Li transference numbers in Li salt/ionic liquid mixtures: does Li drift in the “Wrong” direction?, *Physical Chemistry Chemical Physics* 20 (11) (2018) 7470–7478. doi:10.1039/C7CP08580J.

- [54] K. R. Harris, Comment on “Negative effective Li transference numbers in Li salt/ionic liquid mixtures: does Li drift in the “Wrong” direction?” by M. Gouverneur, F. Schmidt and M. Schönhoff, *Phys. Chem. Chem. Phys.*, 2018, **20**, 7470, Physical Chemistry Chemical Physics 20 (47) (2018) 30041–30045. doi:10.1039/C8CP02595A.
- [55] S. Kucherenko, S. Tarantola, P. Annoni, Estimation of global sensitivity indices for models with dependent variables, *Computer Physics Communications* 183 (4) (2012) 937–946. doi:10.1016/j.cpc.2011.12.020.
- [56] B. Iooss, M. Ribatet, Global sensitivity analysis of computer models with functional inputs, *Reliability Engineering & System Safety* 94 (7) (2009) 1194–1204. doi:10.1016/j.ress.2008.09.010.
- [57] M. Hadigol, A. Doostan, Least squares polynomial chaos expansion: A review of sampling strategies, *Computer Methods in Applied Mechanics and Engineering* 332 (2018) 382–407. doi:10.1016/j.cma.2017.12.019.
- [58] K. Qian, Y. Li, Y.-B. He, D. Liu, Y. Zheng, D. Luo, B. Li, F. Kang, Abuse tolerance behavior of layered oxide-based Li-ion battery during overcharge and over-discharge, *RSC Advances* 6 (80) (2016) 76897–76904. doi:10.1039/C6RA11288A.